Article

TRANSPARENT PROCESS OPEN ACCESS

EMBO reports

AIF inhibits tumor metastasis by protecting PTEN from oxidation

Shao-Ming Shen[1,†], Meng Guo[1,†], Zhong Xiong[1], Yun Yu[1], Xu-Yun Zhao[2], Fei-Fei Zhang[1] & Guo-Qiang Chen[1,3,*]

Abstract

Apoptosis-inducing factor (AIF) exerts dual roles on cell death and survival, but its substrates as a putative oxidoreductase and roles in tumorigenesis remain elusive. Here, we report that AIF physically interacts with and inhibits the oxidation of phosphatase and tensin homolog on chromosome ten (PTEN), a tumor suppressor susceptible for oxidation-mediated inactivation. More intriguingly, we also identify PTEN as a mitochondrial protein and the ectopic expression of mitochondrial targeting sequence-carrying PTEN almost completely inhibits Akt phosphorylation in PTEN-deficient cells. AIF knockdown causes oxidation-mediated inactivation of the lipid phosphatase activity of PTEN, with ensuing activation of Akt kinase, phosphorylation of the Akt substrate GSK-3β, and activation of β-catenin signaling in cancer cells. Through its effect on β-catenin signaling, AIF inhibits epithelial–mesenchymal transition (EMT) and metastasis of cancer cells *in vitro* and in orthotopically implanted xenografts. Accordingly, the expression of AIF is correlated with the survival of human patients with cancers of multiple origins. These results identify PTEN as the substrate of AIF oxidoreductase and reveal a novel function for AIF in controlling tumor metastasis.

Keywords AIF; cancer metastasis; oxidation; PTEN; β-catenin signaling
Subject Category Cancer
DOI 10.15252/embr.201540536 | Received 13 April 2015 | Revised 25 August 2015 | Accepted 26 August 2015 | Published online 28 September 2015
EMBO Reports (2015) 16: 1563–1580

Introduction

Apoptosis-inducing factor (AIF) was originally described as a mitochondrial protein shown to mediate caspases-independent cell death [1]. Upon an apoptotic insult, AIF undergoes proteolysis and is released from mitochondrial intermembrane space, then translocating to the nucleus, where it mediates nuclear morphology of apoptosis such as chromatin condensation and large-scale DNA degradation [2,3]. Beyond its participation in lethal signal transduction, AIF is also regarded as a protein critical for cell survival and required for normal development [4]. Biochemically, human AIF is phylogenetically preserved and structurally homologous to BphA4, a bacterial oxygenase-coupled nicotinamide adenine dinucleotide (NADH)-dependent ferredoxin reductase that has a fold similar to enzymes of the eukaryotic glutathione reductase family [5]. AIF contains two flavin adenine dinucleotide (FAD)-binding domains (residues 128–262 and 401–480), a putative NADH-binding domain (residues 263–400), and a C-terminal domain (residues 481–608) [1]. The oxidoreductase activity of AIF was reported to be absolutely required for mitochondrial energy production and optimal function of the respiratory chain [2]. However, its specific enzymatic functions remain greatly unknown. On the other hand, it has been widely accepted that resisting cell death and reprogramming cell survival and energy metabolism are among biological capabilities acquired during the multistep development of human tumors and play important roles in tumorigenesis [6]. Therefore, we hypothesized that the death and survival-related AIF should exert some roles in the pathogenesis of cancers.

The tumor suppressor gene PTEN (phosphatase and tensin homolog on chromosome ten) plays a critical role in maintaining normal cell activities. It belongs to the tyrosine phosphatase family, but its most prominent role pertains to its lipid phosphatase activity with phosphatidylinositol 3,4,5 trisphosphate (PIP3) as its primary substrate. Since PIP3 is the main cellular product of the class I phosphoinositide 3-kinases (PI3K), PTEN is capable of antagonizing PI3K activity and negatively regulates the PI3K–Akt signaling pathway [7]. The normal activity of PTEN depends on the presence of a highly reactive cysteine (Cys) residue, which is prone to be oxidized [8]. Both endogenous hydrogen peroxide (H_2O_2) and exogenous hydrogen peroxide (H_2O_2) have been shown to cause oxidation of Cys^{124} in the catalytic center of PTEN to form a disulphide bond with Cys^{71}, thereby leading to the reversible inactivation of PTEN phosphatase activity, followed by the increase in Akt phosphorylation [9]. This reversible inactivation of PTEN is commonly seen in cells treated with growth factors that stimulate peroxide production, implying that PTEN responds to mitogens through

1 Department of Pathophysiology, Key Laboratory of Cell Differentiation and Apoptosis of Chinese Ministry of Education, Shanghai Jiao Tong University School of Medicine (SJTU-SM), Shanghai, China
2 Life Sciences Institute, University of Michigan, Ann Arbor, MI, USA
3 Institute of Health Sciences, Shanghai Institutes for Biological Sciences of Chinese Academy of Sciences-SJTU-SM, Shanghai, China
*Corresponding author. Tel/Fax: +86 21 64154900; E-mails: chengq@shsmu.edu.cn; gqchen@sibs.ac.cn
†These authors contributed equally to this work

reduction–oxidation inactivation. Besides directly oxidizing the Cys residue of PTEN, recently, it is also reported that reactive oxygen species (ROS) can inactivate PTEN by indirectly stimulating its phosphorylation and thus gives rise to the activation of the PI3K/Akt signaling pathway [10]. Totally, the persistent abnormal reduction–oxidation status will cause a complete loss of PTEN function. Therefore, it is important that normal cells develop the mechanisms to protect PTEN from ROS-induced inactivation or to re-activate the oxidized PTEN to exert its tumor suppressor function. Although it was reported that peroxiredoxin 1 (Prdx1) protects PTEN from ROS-induced inactivation, thereby suppressing oncogenes-induced transformation [11], and the thioredoxin-interacting protein (Txnip) can re-activate the oxidized PTEN possibly through thioredoxin nicotinamide adenine dinucleotide phosphate oxidase (NAPDH)-dependent reduction in the PTEN disulfide [12], the intracellular mechanisms that protect PTEN from oxidation remain greatly elusive.

Herein, we provide the first demonstration that AIF physically interacts with and inhibits the oxidation of PTEN in cancer cells. Accordingly, the expression of AIF is correlated with the survival of human cancers of multiple origins, and reduced AIF expression causes oxidation-mediated inactivation of the lipid phosphatase activity of PTEN protein together with the activation of β-catenin signaling in cancer cells, through which AIF inhibits epithelial–mesenchymal transition (EMT) and metastasis of cancer cells *ex vivo* and in orthotopically implanted xenografts.

Results

Direct interaction of AIF with PTEN protein

To explore the potential AIF-interacting proteins, human embryonic kidney 293T cells were transfected with the empty or Flag-tagged AIF-expressing plasmids, and cell lysates were immunoprecipitated (IP) by anti-Flag antibody. The precipitates were separated on SDS–PAGE, followed by in-gel digestion and LC–MS/MS analysis (Fig 1A). Totally, 105 AIF-interacting candidates were identified (data not shown), which included four known AIF-interacting proteins: X-linked inhibitor of apoptosis (XIAP) [13], E3 ubiquitin–protein ligase CHIP [14], optic atrophy 1 (OPA1) [15], and mitochondrial import factor CHCHD4 [16]. The interactions of AIF with XIAP and OPA1 were confirmed by co-IP-based immunoblots (Fig 1B), supporting the specificity and effectiveness of our co-IP assay. Of great interest, PTEN protein was among these AIF-interacting proteins, which could also be confirmed by immunoblotting with anti-PTEN antibody (Fig 1B). To consolidate the AIF–PTEN interaction, AIF and/or Flag-PTEN, or hemagglutinin (HA)-PTEN and/or AIF-Flag were exogenously expressed in 293T cells followed by IP with anti-Flag antibody. The results showed that Flag-PTEN could pull down the AIF, and AIF-Flag precipitated HA-PTEN (Fig 1C and D). The interaction between endogenous AIF and PTEN was also found in colon cancer cell line SW620 cells but not in PTEN-deficient prostate cancer cell line LNCaP cells (Fig 1E). Furthermore, glutathione S-transferase (GST) pull-down assay showed that the *in vitro* recombinant GST-tagged AIF, but not GST alone significantly pulled down His-tagged PTEN (Fig 1F), supporting a direct interaction of AIF with PTEN.

Domain mapping of AIF–PTEN interaction

To map the domains of PTEN involved in its interaction with AIF, the Flag-tagged N-terminal fragment with phosphatase activity (PTEN-N) and C-terminal fragment (PTEN-C) of PTEN (Fig 1G) were transfected into 293T cells together with AIF, followed by co-IP with anti-Flag antibody. As depicted in Fig 1H and I, PTEN-N but not PTEN-C pulled AIF down, and anti-AIF antibody pulled PTEN-N down but not PTEN-C, proposing the N-terminal phosphatase domain of PTEN is required for its interaction with AIF protein.

To define the PTEN-binding domain of AIF, the *in intro* recombinant GST-tagged full-length AIF (AIF-FL) and its three fragments, including the N-terminal (AIF-N), C-terminal (AIF-C), and middle (AIF-M) fragments (Fig 1J), were, respectively, incubated with cell lysates from the Flag-PTEN-N-transfected 293T cells, and GST pull-down assay revealed that GST-AIF-M corresponding to the oxidoreductase domain of AIF, but not GST-AIF-C, most potently pulled down PTEN-N (Fig 1K, left panel). AIF gene also expresses several short splice variants such as AIFshort (AIFsh), AIFsh2, and AIFsh3 (Fig 1J), as reviewed [2]. Although an earlier work reported that most cells and tissues did not express the AIFsh3 [17], our RT–PCR assays showed that SW620 cells could express AIFsh3 besides AIFsh and AIFsh2 mRNA (Fig EV1A), and immunoblots with an antibody specifically against residues 151–168 of AIF, which can detect AIFsh2 and AIFsh3 besides AIF-FL, showed that SW620 cells and other several cells expressed AIF-FL, AIFsh2, and AIFsh3 to a different degree, with AIFsh3 protein to a lowest degree (Fig EV1B). Moreover, full-length AIF and AIFsh2 were localized in the mitochondria, while AIFsh3, which is missing the N-terminal mitochondrial localization sequence (MLS), mainly expressed in the cytoplasm of SW620 cells (Fig 1L) [18]. More intriguingly, all three AIF short isoforms interacted with PTEN-N, assessed by GST pull-down (Fig 1K, middle panel) and co-IP assays (Fig EV1C). Because all three short isoforms carry one FAD domain, we further detected the potential interaction of PTEN-N with FAD1 and/or FAD2 domains-deleted AIF mutants. The results showed that FAD1- or FAD2-deleted AIF mutant still interacted with PTEN-N, which was completely lost when both FAD1 and FAD2 were deleted (Fig 1K, right panel). Collectively, our data propose that two FAD-binding domains of AIF are required for its interaction with PTEN.

Mitochondrial localization of PTEN

The AIF is synthesized in the cytosol and transported into mitochondria to reside in the intermembrane space where the MLS is removed [1,2], while PTEN was initially assumed to be exclusively localized to the cytoplasm and exerts its role as a lipid phosphatase at the plasma membrane. Although it is well documented that a pool of PTEN protein is localized to the nucleus and gains new functions [19], it is controversial whether PTEN is localized in mitochondria, especially on the outer membrane of mitochondria or intermitochondria [20–23]. Therefore, we also continued to decide whether PTEN is also localized in mitochondria. Toward this goal, we fractionated the cytoplasms of SW620 cells into 12 fractions by 8.5–60% sucrose gradient. As depicted in Fig 2A, PTEN could be clearly found in mitochondrial fractions along with AIF and cytochrome *c* oxidase-IV (Cox-IV). In line with the fact, PTEN could also be found in mitochondria fractions of SW620 and DU145 cells purified by

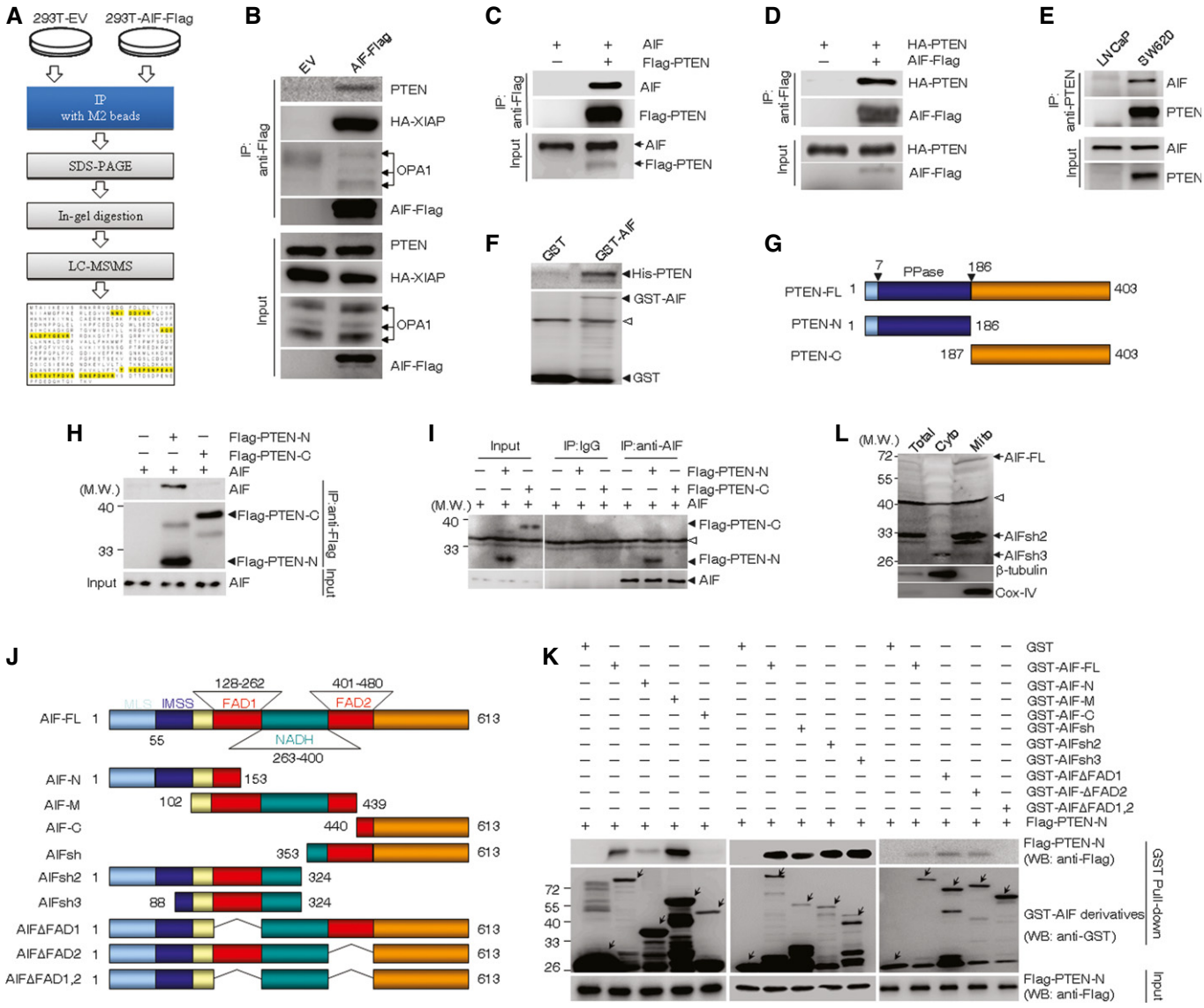

Figure 1. AIF and its isoforms interact with PTEN.

A Workflow for identification of AIF-interacting proteins.

B–D 293T cells were transfected with AIF-Flag and HA-tagged XIAP (B), AIF and Flag-tagged PTEN (C), or Flag-tagged AIF and HA-tagged PTEN (D). Co-IP was performed with M2 beads followed by Western blots for the indicated proteins. Note: Input blot in (C) was initially detected with a rabbit anti-AIF antibody followed by HRP-conjugated anti-rabbit IgG. Then, the blot without stripping was used to detect Flag-PTEN with a mouse anti-Flag antibody followed by HRP-conjugated anti-mouse IgG.

E Cell lysates from LNCaP and SW620 cells were immunoprecipitated with anti-PTEN antibody, and precipitates/input were detected by Western blots.

F Bacterially expressed GST or GST-AIF protein was incubated with His-PTEN, followed by GST pull-down and Western blots for His and GST. The empty arrowhead points to a non-specific band.

G–I Schematic illustrations of PTEN fragments (G). Flag-PTEN-N or Flag-PTEN-C were transfected into 293T cells together with AIF, followed by co-IP with M2 beads (H) or anti-AIF antibody/IgG (I). The precipitates were detected by Western blots. The empty arrowhead points to a non-specific band. PPase, phosphatase.

J Schematic illustrations of AIF fragments, isoforms, and deleted mutants. MLS, mitochondrial localization signal; IMSS, intermembrane space-targeting signal.

K GST alone or GST fusion proteins were incubated with extracts prepared from 293T cells transfected with Flag-PTEN-N, and GST pull-downs were analyzed by Western blots with antibodies against Flag and GST. Arrows point to the indicated GST or GST fusion proteins.

L SW620 cells were separated into cytosol (Cyto) and mitochondria (Mito) fractions, followed by Western blots. The empty arrowhead indicates an unknown band.

ultracentrifugation in a density gradient medium of iodixanol (Fig 2B). Further, the purified mitochondria were incubated with trypsin and/or Triton X-100, as trypsin only digests outer membrane proteins and contaminating cytosolic proteins due to mitochondrial membrane protection which is disrupted by the presence of Triton X-100. The results showed that Bcl-X_L, which is localized on the outer membrane of mitochondria, was degraded, whereas PTEN was resistant to trypsin, like mitochondria-resided AIF and mitochondrial complex I subunit NADH–ubiquinone oxidoreductase 30 kDa subunit (Ndufs3). When trypsin was added

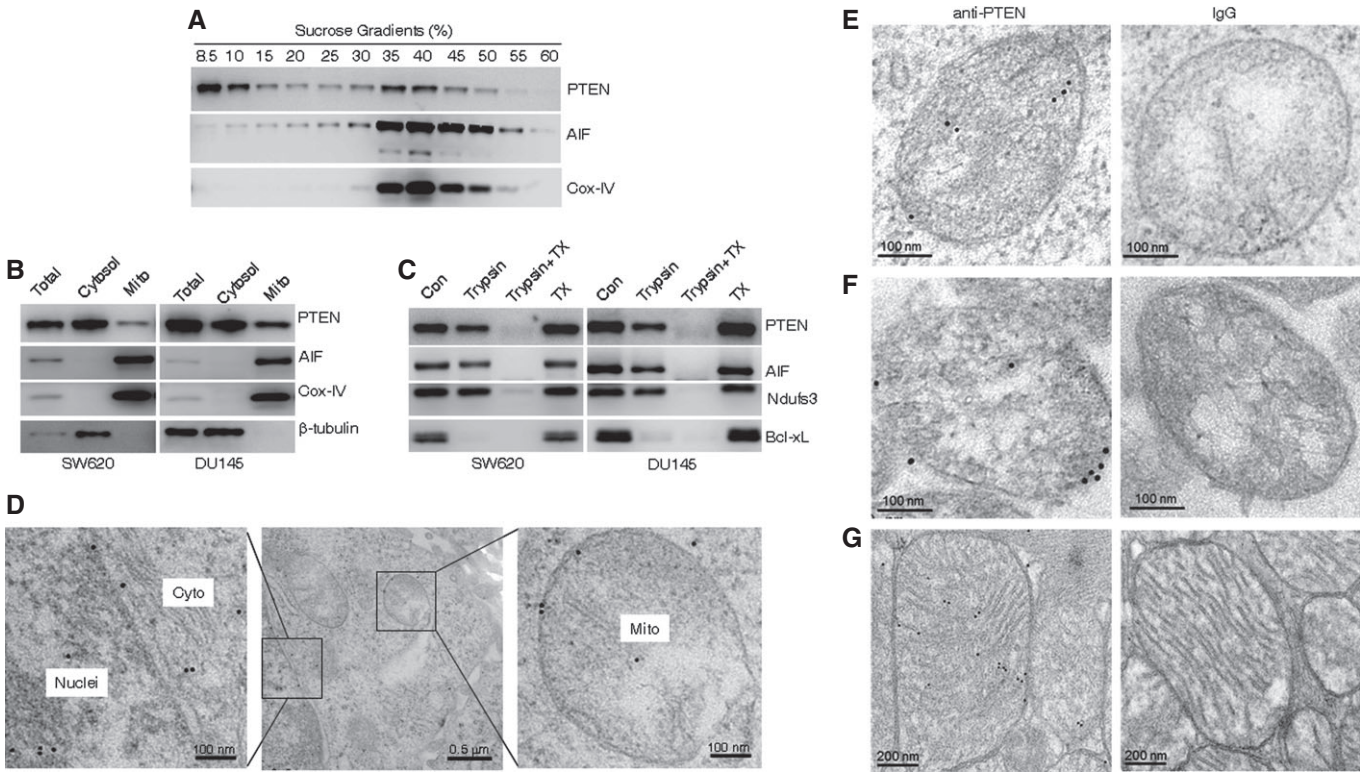

Figure 2. PTEN is also a mitochondrial protein.

A Cytoplasms of SW620 cells were fractionated by 8.5–60% sucrose gradient centrifugation, and the resultant fractions were analyzed by Western blots for proteins as indicated.

B The cytosol and mitochondria (mito) were fractionated from SW620 and DU145 cells by ultracentrifugation in a density gradient medium of iodixanol, and the expressions of proteins as indicated in whole-cell lysates and fractions (containing 5 μg of protein each) were examined by Western blots.

C The purified mitochondria of SW620 and DU145 cells were treated with 0.25 μg/μl trypsin and/or 1% Triton X-100 (TX), followed by Western blots for the proteins as indicated.

D SW620 cells labeled with anti-PTEN antibody were stained with gold-conjugated secondary reagent and analyzed by electron microscopy. Cyto, cytosol; Mito, mitochondria.

E–G Mitochondrion in intact SW620 cells (E), isolated mitochondrion from SW620 cells (F), and mitochondria in mouse cardiac muscle (G) labeled with anti-PTEN antibody or IgG were stained with gold-conjugated secondary reagent and observed by electron microscopy.

to mitochondria in the presence of Triton X-100, all of these proteins were degraded (Fig 2C). To consolidate that PTEN is an intramitochondrial protein, immunoelectron microscopy assay was performed with an antibody specifically against PTEN with non-related IgG as a negative control. As depicted in Fig 2D and E, the anti-PTEN antibody could label mitochondria besides cytosol and nuclei within intact SW620 cells. The specific staining of PTEN could also be seen in isolated mitochondria from SW620 cells (Fig 2F) and mitochondria within freshly harvested mouse cardiac muscle (Fig 2G). Thus, all these data strongly support that PTEN is also a mitochondrial protein.

Oxidoreductase activity of AIF on PTEN

Then, we transfected a mitochondrial targeting sequence-carrying PTEN (mito-PTEN) into PTEN-deficient prostate cancer PC3 cells. As depicted in Fig 3A, all mito-PTEN protein was localized into mitochondria, as assessed by co-localization with mitochondrial protein Cox-IV. More intriguingly, the ectopically expressed mito-PTEN was capable of significantly inhibiting Akt phosphorylation (Fig 3B), suggesting that mitochondrial PTEN can signal to Akt. Mitochondria are an important source of ROS during ATP production, while PTEN is easily inactivated by oxidation. In particular, a key hallmark of cancer cells is unrestrained growth [6]. Because ROS generation is a by-product of cell growth, cancer cells sustain a much higher level of ROS production compared to normal cells, and thus, it was believed that cancer cells are characterized with high status of oxidative stress [24,25]. Therefore, we attempted to investigate whether and how AIF regulates PTEN. Consistent with the previous report [8], bacterially expressed PTEN was oxidized to different extent including a band around 70 kDa during the *in vitro* purification so that the reduced form of PTEN (~60 kDa) was barely detectable under non-reducing condition (Fig EV2A and B). Upon exposure to exogenous H_2O_2, these *in vitro* purified PTEN appeared to be highly oxidized, with the disappearance of the oxidized band around 70 kDa under non-reducing condition (Fig EV2B), for which a potential explanation could be aggregation of oxidized forms that is exacerbated in the presence of H_2O_2 to an extent where the oxidized PTEN was difficult or no longer entered the gel. However, dithiothreitol (DTT) treatment resulted in the

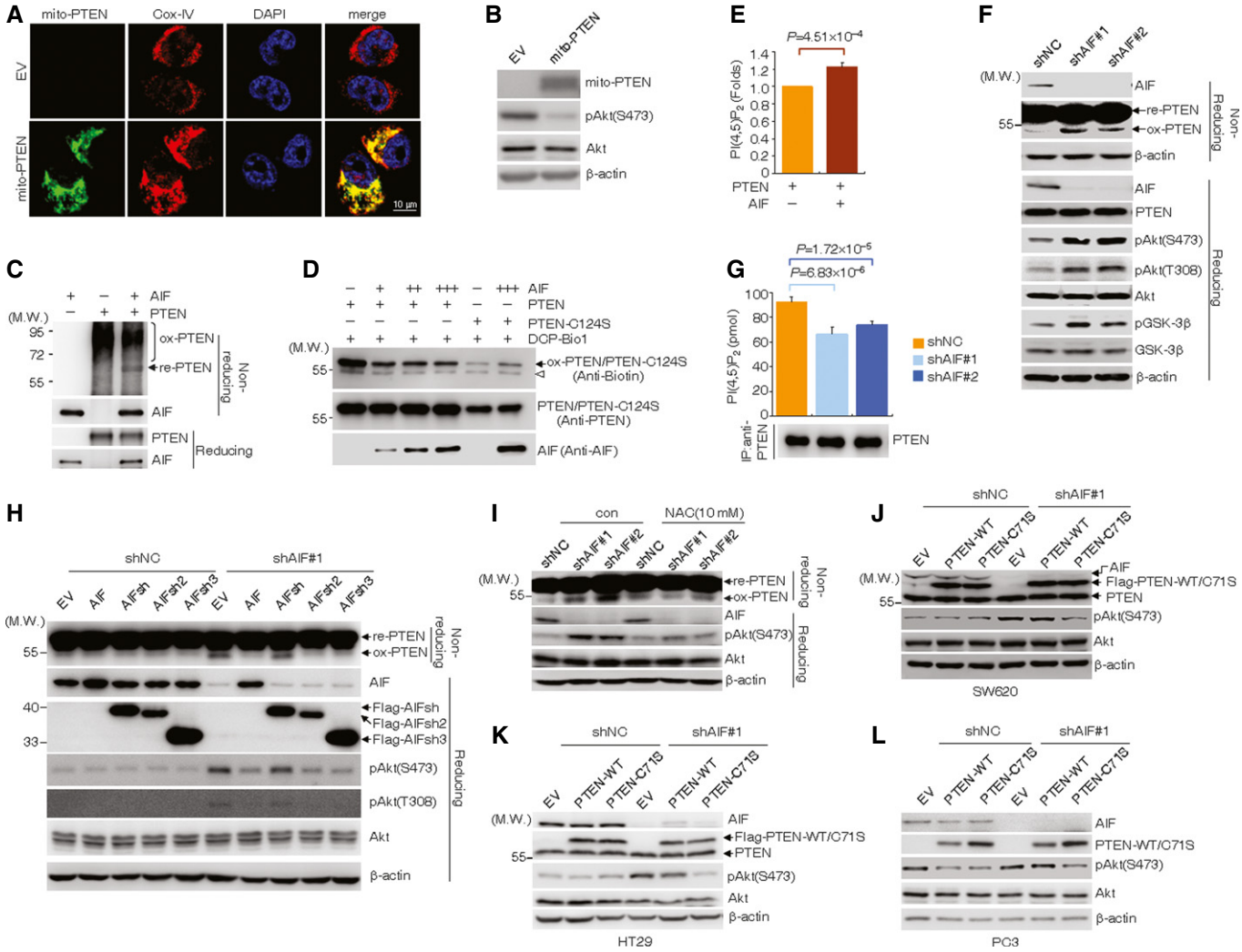

Figure 3. AIF prevents oxidative inactivation of PTEN.

A, B PC3 cells were transfected with empty vector (EV) or mito-PTEN. Immunofluorescence staining of mito-PTEN and Cox-IV with re-staining of DAPI (A) and Western blots for the indicated proteins (B) were performed. Scale bar represents 10 μm.

C The recombinant PTEN protein (50 ng) was incubated with recombinant AIF (50 ng) in the presence of 200 μM NADH at 4°C for 1 h. The mixtures were prepared under non-reducing or reducing condition and blotted for the indicated proteins. "ox" indicates oxidized protein and "re" indicates the reduced band of PTEN.

D The recombinant PTEN or PTEN-C71S protein was incubated with recombinant AIF in the presence of 200 μM NADH at 4°C for 1 h, followed by incubation with 500 μM DCP-Bio1 in the presence of 50 mM indole-3-acetic acid (IAA) at 4°C for 1 h. The mixtures were prepared under reducing condition and blotted for biotin (top), PTEN (middle), or AIF (bottom). "ox" indicates DCP-Bio1 labeled oxidized protein. The empty arrowhead indicates a non-specific band.

E The recombinant PTEN (0.5 μg) protein was incubated in the presence or absence of recombinant AIF (4 μg), and relative PTEN phosphatase activity was determined. Data represent means and s.d of three independent experiments. Two-sided unpaired *t*-test.

F Cell lysates from shNC- or shAIF-infected SW620 cells were prepared under reducing or non-reducing condition and analyzed by Western blots for the indicated proteins. "ox" indicates oxidized protein and "re" indicates reduced PTEN.

G The shNC- or shAIF-infected SW620 cells were subjected to IP using anti-PTEN antibody. Equal PTEN protein amount was confirmed by Western blots, and data represent means and s.d of three independent experiments. Two-sided unpaired *t*-test.

H EV, AIF, and Flag-tagged AIFsh, AIFsh2, or AIFsh3 were expressed in shNC- or shAIF#1-infected SW620 cells. Cell lysates were prepared under reducing or non-reducing conditions and analyzed by Western blots for the indicated proteins. "ox" indicates oxidized protein and "re" indicates reduced PTEN.

I The shNC- or shAIF-infected SW620 cells were treated with or without 10 mM NAC for 2 h. Lysates were prepared under reducing or non-reducing condition and analyzed by Western blots for the indicated proteins. "ox" indicates oxidized protein and "re" indicates reduced PTEN.

J–L EV, PTEN-WT, or PTEN-C71S was transfected into shNC- or shAIF#1-infected SW620 (J), HT29 (K), or PC3 (L) cells. Lysates were analyzed by Western blots for the indicated proteins.

appearance of a single band of ~60 kDa PTEN (Fig EV2A). The fact that the putative oxidoreductase domain of AIF interacts with the phosphatase domain of PTEN prompted us to ask whether AIF regulates the redox state of PTEN. Indeed, when the *in vitro* purified PTEN was incubated with the recombinant AIF under non-reducing condition, a band matching with the reduced form of PTEN could be clearly seen (Figs 3C and EV2B and C). Of note, the NADH oxidase domain-deleted AIF mutant, AIFΔNADH, failed to

generate the reduced form of PTEN (Fig EV2C). It was reported that H_2O_2-mediated PTEN oxidation resulted in an intramolecular disulfide bond formed between Cys^{124} and Cys^{71}, and mutation of either site resists oxidation by H_2O_2 [9]. Hence, the recombinant PTEN was incubated with escalating concentrations of AIF with PTEN-C124S as a control, followed by probing with DCP-Bio1, a biotin-tagged probe which links covalently to oxidized cysteine and has been used to monitor oxidized proteins [26]. The results showed that AIF decreased a biotinylated band matched with PTEN with a dose independence, while the PTEN-C124S mutant presented few oxidation (Fig 3D). It is well known that PTEN is inactivated by oxidation in the N-terminal phosphatase domain [9]. In line with this, AIF increased PTEN lipid phosphatase activity *in vitro* (Fig 3E).

To address whether AIF regulates intracellular PTEN oxidation, two pairs of shRNAs (shAIF#1 and shAIF#2) specifically against AIF were used to knockdown AIF expression, together with non-specific scramble shRNA (shNC) as a negative control. These shRNAs but not shNC significantly silenced AIF expression (Fig 3F). Consistent with a previous report [27], the mitochondrial complex I subunits NADH–ubiquinone oxidoreductase 75 kDa subunit (Ndufs1) and Ndufs3 were also decreased in SW620 cells with AIF knockdown (Fig EV2D), suggesting the effectiveness of AIF knockdown. AIF knockdown failed to affect the expression of PTEN protein (Fig 3F). However, when Western blots were performed under non-reducing condition, the oxidative PTEN was dramatically increased by AIF loss in SW620 (Fig 3F), as well as in colon cancer HT29 (Fig EV2E) and prostate cancer DU145 cells (Fig EV2F). In accordance, AIF knockdown inhibited PTEN lipid phosphatase activity in SW620 cells (Fig 3G), together with the increased phosphorylations of Akt on serine 473 (S473) and threonine 308 (T308), and of GSK-3β, an Akt substrate (Fig 3F). The same phenomena were also obtained in HT29 and DU145 cells (Fig EV2E and F), but not in PTEN-deficient PC3 and LNCaP cells (Fig EV2G). Notably, AIF knockdown appeared to reduce Akt-S473 and GSK-3β phosphorylations in the PC3 cells, suggesting that additional factors impinge on the functional connections between AIF, Akt, and GSK3-3β in the PTEN-deficient cells. Importantly, AIF overexpression effectively reversed AIF knockdown-induced PTEN oxidation and Akt phosphorylation (Fig 3H).

Consistent with the previous reports [9], H_2O_2 incubation induced PTEN oxidation (Fig EV2H and I). More intriguingly, the exogenous H_2O_2-increased PTEN oxidation could also be significantly enhanced by AIF knockdown (Fig EV2H and I), while treatment of N-acetyl-l-cysteine (NAC), a H_2O_2 scavenger, not only prevented PTEN from oxidation, but also abolished the AIF knockdown-induced Akt activation (Fig 3I). On the other hand, AIF knockdown did not increase the intracellular ROS level (Fig EV2J), precluded the possibility of increased ROS-induced PTEN oxidation in AIF knockdown cells. Of note, treatment with low concentration of H_2O_2 did not induce the nuclear translocation of AIF (Fig EV2K) and it also did not impact on the AIF–PTEN interaction (Fig EV2L). All these data support that AIF can protect PTEN from the *in vivo* oxidative inactivation in either endogenous or exogenous oxidative stress. As reported [17], AIFsh2 and AIFsh3 but not AIFsh contain the oxidoreductase domain of AIF. Although PTEN interacts with all these short isoforms, our results showed that, like AIF, AIFsh2 and AIFsh3 but not AIFsh could rescue AIF knockdown-induced PTEN oxidation and Akt activation (Fig 3H), further supporting that the effects of AIF on PTEN are enzymatic.

Although PTEN oxidation has been proved to be crucial for its activity, here we noticed that only a small fraction of PTEN was oxidized compared to total PTEN upon AIF knockdown. Actually, the same phenomenon was also observed with direct H_2O_2 exposure. As shown in Fig EV2M, H_2O_2 induced a fast and transient oxidation of a small fraction of PTEN accompanied with increased Akt phosphorylation, which could be antagonized by NAC pretreatment, proposing that the oxidation of a part of PTEN can disrupt the activity of all PTEN, although its mechanisms remain to be illustrated. On the other hand, Cys^{124} is localized in the phosphatase activity center of PTEN, and the C124S mutant completely abolishes PTEN activity [28,29]. However, the C71S mutant still keeps the partial activity of PTEN relative to its wild-type form [30]. Here, we showed that the PTEN C71S mutant still interacted with AIF (Fig EV2N), suggesting that the cysteine is dispensable for PTEN–AIF interaction. Thus, we tested whether the C71S mutant reversed AIF knockdown-enhanced oxidative inactivation of PTEN. To this end, we introduced PTEN-WT or PTEN-C71S into PTEN-deficient PC3 cells and found that both proteins, especially PTEN-WT, inhibited Akt phosphorylation (Fig EV2O). When these cells were exposed to H_2O_2, a small fraction of PTEN-WT but not PTEN-C71S protein was oxidized (Fig EV2O). Meanwhile, H_2O_2 counteracted the PTEN-WT but not PTEN-C71S mutant-induced inhibition of Akt phosphorylation (Fig EV2O), indicating the effectiveness of PTEN-C71S in resisting its oxidation and inactivation. In accordance, when PTEN-WT and PTEN-C71S were ectopically expressed in SW620 and HT29 cells with AIF knockdown, PTEN-C71S mutant but not PTEN-WT rescued AIF knockdown-induced Akt phosphorylation in these two cell lines (Fig 3J and K). Also, the ectopically expressed PTEN-WT but not PTEN-C71S failed to inhibit Akt phosphorylation in AIF-silenced PC3 cells (Fig 3L). Cumulatively, all of these data support the involvement of AIF oxidoreductase activity in the regulation of PTEN/Akt/GSK-3β signaling.

Activation of WNT/β-catenin signaling upon AIF loss

The Akt-mediated phosphorylation inactivates GSK-3β, which leads to the accumulation and nuclear translocation of β-catenin, one of the most important substrates of GSK-3β [31]. Indeed, there was abundant nuclear β-catenin in AIF knockdown cells but not in shNC cells (Fig 4A and B). Nuclear β-catenin facilitates the transcriptional activation of WNT/β-catenin signaling in complex with transcriptional factor lymphoid enhancer-binding factor-1/T-cell factor-1 (LEF/TCF) [32,33]. To monitor the activation of WNT/β-catenin signaling, shAIF#1-, shAIF#2-, and shNC-infected SW620 cells were transfected with LEF/TCF-responsive promoter Topflash luciferase (containing two sets of three copies of the LEF/TCF-binding sites) and its mutant Fopflash. The results showed that AIF silencing significantly activated Topflash but not Fopflash (Fig 4C), indicating the activation of WNT/β-catenin transcription in AIF knockdown cells. Consistently, the mRNA levels of all six WNT/β-catenin target genes tested (DKK1, LEF1, MMP7, TCF4, AXIN2, and ID2) presented the upregulated expression upon AIF knockdown in SW620 (Fig 4D) and HT29 cells (Fig EV3A). The increased expression of Axin2 in AIF knockdown SW620 cells was also confirmed on the protein level (Fig EV3B). Vice versa, the overexpression of AIF downregulated

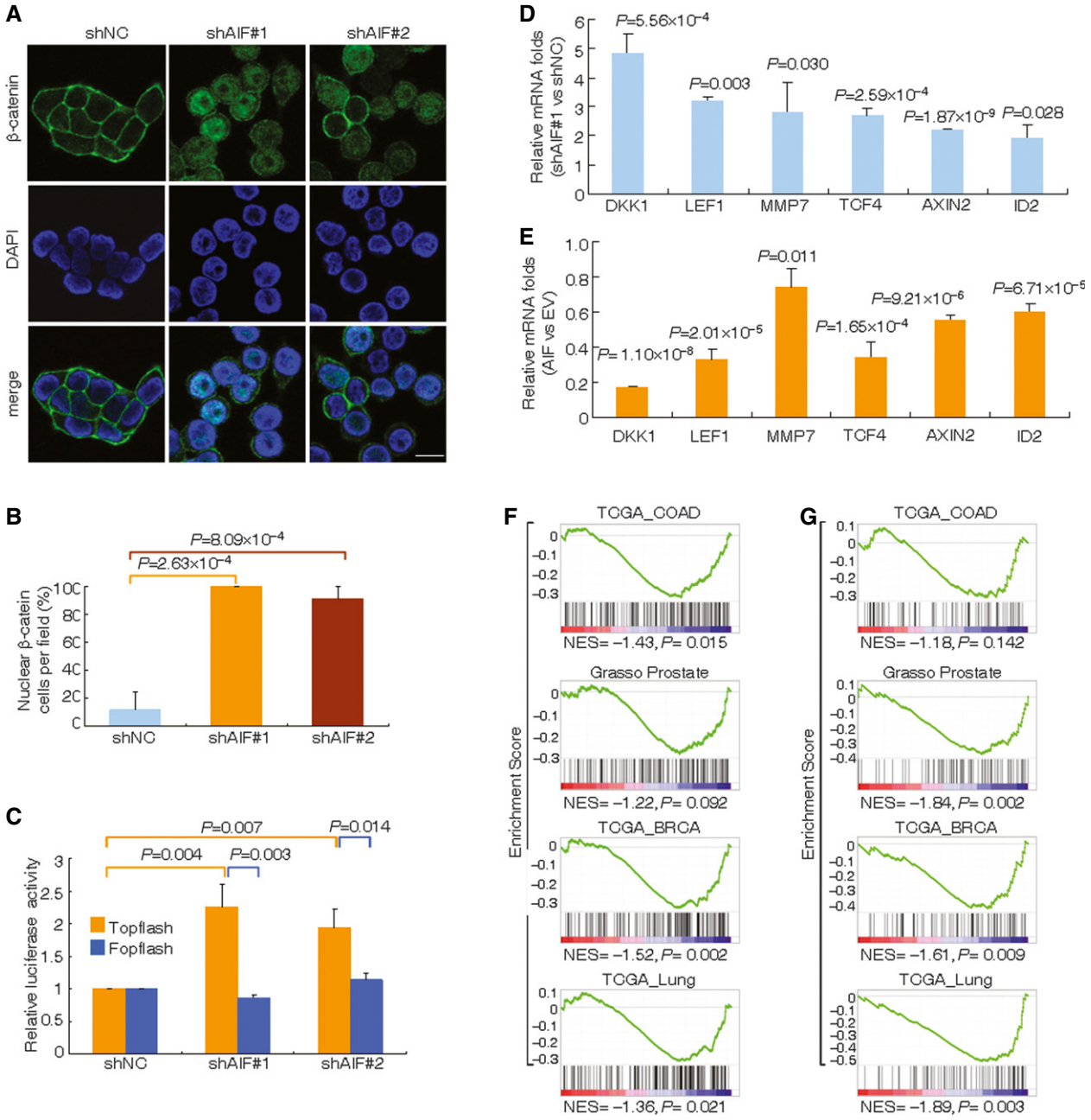

Figure 4. AIF negatively regulates WNT/β-catenin signaling.

A, B Immunofluorescence staining of β-catenin with re-staining of DAPI in shNC- or shAIF-infected SW620 cells with scale bar representing 10 μm (A). The percentage of cells with nuclear β-catenin was calculated (B).

C shNC- or shAIF-infected SW620 cells were transiently transfected with Topflash or Fopflash firefly luciferase reporter plasmids. Twenty-four hours later, relative luciferase activities against shNC cells were determined.

D The folds of relative mRNA levels of the indicated genes against shNC-infected cells were quantified by quantitative real-time PCR in shAIF#1-infected SW620 cells.

E The folds of relative mRNA levels of indicated genes against EV-infected cells were quantified by quantitative real-time PCR in AIF-overexpressed SW620 cells.

F, G GSEA data showing the negative correlations of AIF with KEGG WNT/β-catenin signaling pathway gene set (F) and the gene set of 78 WNT/β-catenin signaling target genes (G) in four datasets as described in the text. *y*-axis: value of the ranking metric; *x*-axis: the rank for all genes. The graph on the bottom of each panel represents the ranked, ordered, non-redundant list of genes. Genes on the far left (red) most positively correlated with AIF, and genes on the far right (blue) most negatively correlated with AIF. On each panel, the vertical black lines indicate the position of each of the genes of the studied gene set in the ordered, non-redundant dataset. The green curve corresponds to the ES (enrichment score) curve, which is the running sum of the weighted enrichment score obtained from GSEA software. NES, normalized enrichment score.

Data information: In (B–E), data represent means and s.d of three independent experiments. Two-sided unpaired *t*-test.

these target genes (Fig 4E), and both AIF-FL and AIFsh3 rescued the AIF knockdown-induced activation of Wnt/β-catenin transcription (Fig EV3C). Considering previous reports showing that none of these genes are under sole control of WNT/β-catenin signaling [34,35], we knocked down β-catenin with a pair of shRNA specially against β-catenin (shβ-catenin#2) in AIF-silenced cells and found that β-catenin knockdown almost completely blocked AIF silencing-induced expressions of all six genes (Fig EV3D), proposing the role of the activated β-catenin in the AIF knockdown-mediated events. In addition, gene set enrichment analysis (GSEA) with two human WNT/β-catenin signaling pathway gene sets in four independent microarray datasets (TCGA Colon Adenocarcinoma, TCGA Breast Invasive Carcinoma, TCGA Lung, and Grasso Prostate [36]), confirmed the inverse correlation between AIF and WNT/β-catenin signaling target genes (Fig 4F and G, Tables EV1 and EV2). Thus, we conclude that AIF knockdown results in the activation of β-catenin signaling.

AIF loss activates WNT/β-catenin signaling through oxidative inactivation of PTEN

To address whether AIF regulates WNT/β-catenin signaling through PTEN, we knocked down AIF and/or PTEN in SW620 cells (Fig 5A). AIF or PTEN silencing increased, while their combined knockdown did not further enhance, expressions of WNT/β-catenin signaling target genes (Fig 5B). Furthermore, LY294002, an inhibitor of the PI3K/Akt pathway, significantly antagonized AIF knockdown-induced expressions of all six WNT/β-catenin signaling target genes tested (Fig 5C). Moreover, NAC treatment (Fig 5D) and overexpression of the PTEN-C71S mutant but not wild-type PTEN (Fig 5E) reversed AIF knockdown-induced expressions of WNT/β-catenin signaling target genes. Cumulatively, all these data propose that PTEN oxidative inactivation mediates AIF knockdown-activating WNT/β-catenin signaling.

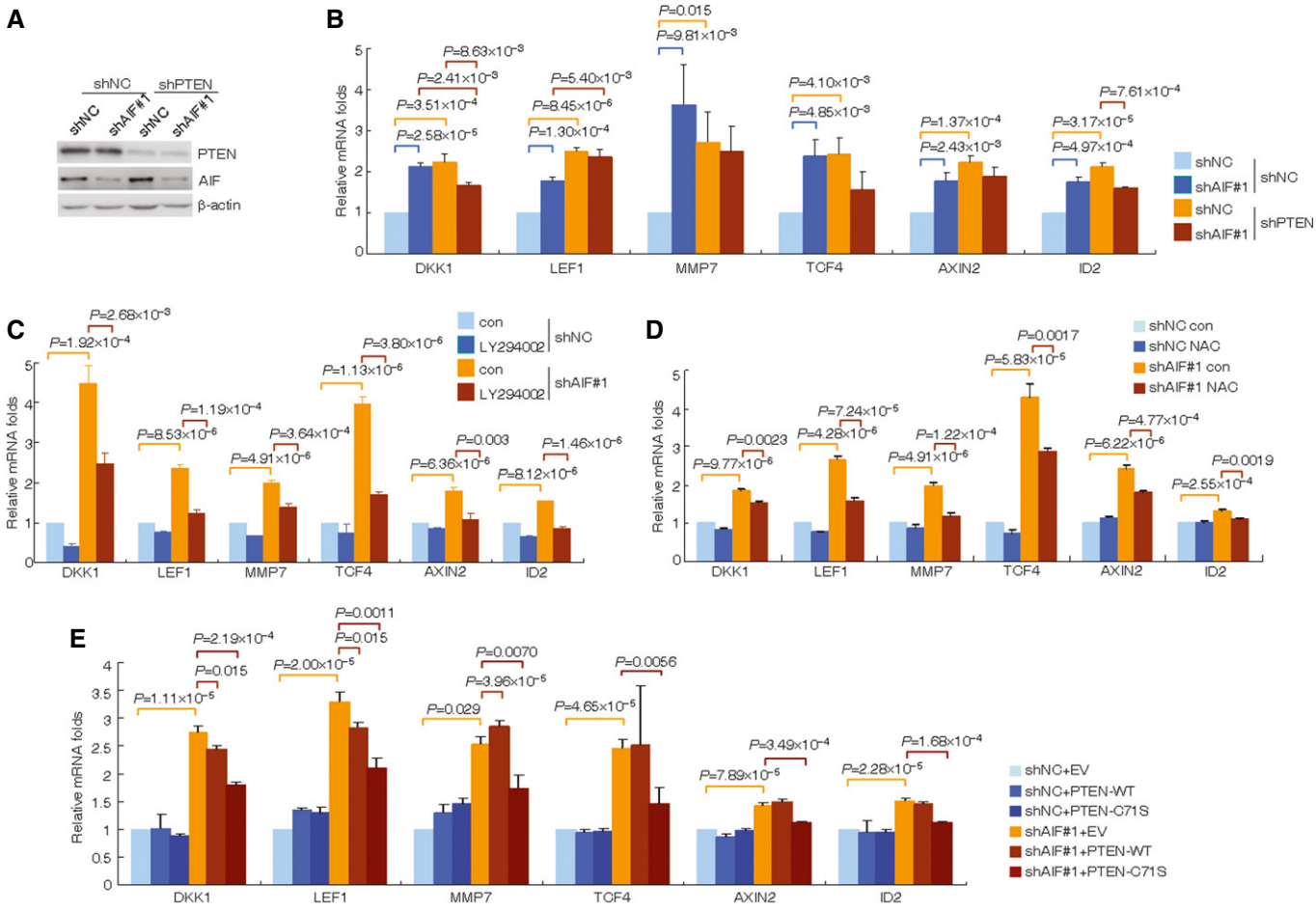

Figure 5. AIF knockdown activates WNT/β-catenin signaling through oxidative inactivation of PTEN.

A, B Western blots for the indicated proteins (A) and quantitative real-time PCR for mRNA levels of the indicated genes (B) in shNC- or shAIF-infected SW620 cells with or without PTEN knockdown. Data represent means and s.d of three independent experiments. Two-sided unpaired *t*-test.

C, D The quantitative real-time PCR for mRNA levels of the indicated genes in LY294002- (C) or NAC-treated (D) SW620 cells with or without AIF knockdown. Data represent means and s.d of three independent experiments. Two-sided unpaired *t*-test.

E EV, PTEN-WT, or PTEN-C71S was transfected into shNC- or shAIF#1-infected SW620 cells. Quantitative real-time PCR for mRNA levels of the indicated genes was performed. Data represent means and s.d of three independent experiments. Two-sided unpaired *t*-test.

AIF knockdown induces EMT through activating β-catenin signaling

The activation of β-catenin signaling has been reported to induce the EMT of cancer cells. Of great interest, upon AIF knockdown in SW620 cells, the mRNA and/or protein levels of the epithelial markers E-cadherin and plakoglobin dramatically decreased, and those of the mesenchymal markers fibronectin and vimentin increased (Fig 6A and B). In line with these biochemical alterations, SW620 cells with AIF knockdown exhibited a spindle-like, fibroblastic morphology compared to the typical cobblestone-like appearance of shNC-infected cells (Fig 6C). Immunofluorescence staining of E-cadherin and vimentin confirmed these EMT-associated shifts (Fig 6D). Considering that some previous reports showed that SW620 cells have at least a partially mesenchymal character, which may be reflected in the heterogeneous appearance of these cells that present with different morphologies in culture [37], we also detected the potential EMT-inducing effect of AIF knockdown in two other cancer cell lines, HT29 and DU145 cells, without WNT/β-catenin pathway activating mutations. The results demonstrated that, like seen in SW620 cells, AIF knockdown could also trigger these two cell lines to undergo EMT (Fig EV4A and B). GSEA with TCGA Colon Adenocarcinoma indicated that AIF negatively correlated with two distinct EMT-related gene signatures [38,39], further suggesting that AIF loss induces a pervasive and sustained EMT signaling program (Fig 6E). Considering that colorectal tumor preparations could be contaminated by stromal cells and that EMT signature gene expression was due to the stromal contaminants [40], we also examined the correlation between AIF and E-cadherin by immunohistochemical analysis (IHC) in a group of colon cancer tissues (Table EV3) and confirmed that the expression of AIF is indeed positively correlated with that of E-cadherin (Fig EV4C–E).

We also detected the expressions of the main EMT activators including ZEB1, Twist, Snail, and Slug upon AIF knockdown in SW620 cells, and results showed that among these four activators, the expression of only ZEB1, another target gene of WNT/β-catenin signaling [41], was elevated by AIF knockdown (Figs 6A and B, and EV4F). Of note, it appeared that the increase in ZEB1 protein was more significant than its mRNA upon AIF knockdown (Fig 6A and B). We further addressed whether AIF knockdown-triggered EMT is a result of WNT/β-catenin signaling activation, and we infected two pairs of shRNA against β-catenin (shβ-catenin#1 and shβ-catenin#2) in AIF knockdown cells, which effectively silenced the β-catenin expression (Fig 6F). These two shRNAs almost completely reversed the ZEB1 protein increase and EMT program upon AIF silencing (Fig 6F and G). The re-expression of the PTEN-C71S mutant but not PTEN-WT reversed the EMT program, including EMT marker expression (Fig 6H and I) and morphological changes (Fig 6J). Taken together, our results indicate that AIF knockdown induces EMT through WNT/β-catenin signaling activation caused by PTEN oxidative inactivation.

AIF loss promotes tumor metastasis in xenografts and *in vitro* models of cancers

Besides the induction of EMT, most of the WNT/β-catenin signaling target genes tested above, especially TCF4, LEF1, and MMP7, have been implicated to play strong roles in migration, invasion, or cancer metastasis [42–44]. We thus investigated whether AIF regulated these cellular activities. Indeed, AIF knockdown cells exhibited enhanced mobility by a scratch wound-healing assay (Fig 7A) and increased invasiveness by Matrigel-coated Boyden chamber invasion assay (Fig 7B and C). We then subcutaneously injected shNC- or shAIF#1-infected SW620 cells into nude mice (Fig EV5A), where subcutaneous growth of shAIF#1-infected SW620 cells was slower compared with that of shNC-infected ones, although no statistical significance was found (Fig EV5B). Fifteen days post-inoculation, one subcutaneous tumor from each group was harvested, followed by Western blots showing that shAIF#1 still knocked down AIF expression (Fig EV5C). These subcutaneous tumors were cut into pieces (approximately 2 mm in diameter) and were sutured onto the cecum wall of mice. These mice with orthotopic implantations were sacrificed when they developed signs of distress. At that time, shNC- and shAIF#1-infected SW620 cells had generated colon tumors of equivalent sizes (Fig EV5D). However, shAIF#1 colon tumors showed increased Akt and GSK-3β phosphrolation and β-catenin nuclear localization, and decreased E-cadherin expression compared to shNC tumors (Fig 7D and E). Histopathologic observations showed that shAIF#1-infected SW620 colon tumors showed substantially increased local invasion (Fig EV5E). Intriguingly, 10 of 19 mice bearing SW620-shAIF#1 colon tumors developed more hepatic metastatic nodules, which could be seen only in one of SW620-shNC tumor-bearing mice (Fig 7F and G), indicating the enhanced ability of AIF-deficient cells to undergo hepatic metastasis. We also confirmed that, among all the general metastasis-related genes as reviewed [45], WNT/β-catenin target gene LEF1 was most significantly regulated (Fig EV5F and G), supporting the specific role of WNT/β-catenin signaling in AIF knockdown-induced metastasis. Moreover, re-expression of PTEN-C71S mutant almost completely reversed the effect of AIF knockdown on the development of liver metastasis of splenically injected SW620 cells (Fig 7H and I), indicating that the metastasis-promoting role of AIF knockdown is mediated by PTEN oxidation.

To consolidate the role of AIF in metastasis, we also injected GFP-luciferase-labeled colon cancer HT29 cells with or without AIF knockdown into the spleen of mice (Figs 7J and EV5H). Bioluminescent imaging monitoring revealed that animals injected with shAIF#1- and shAIF#2-infected HT29 cells showed enhanced metastatic outgrowth in the livers 4 weeks post-injection (Fig 7K), and histological analyses indicated more than ten-fold increase in the numbers of metastatic liver nodules produced by AIF-silenced HT29 cells than control cells (Fig 7L and M). All these data support that knockdown of AIF expression promotes the metastasis of cancer cells.

Low AIF expression is correlated with poor outcome of cancer patients

Finally, we detected AIF protein by IHC in tumor tissues from 82 cases of patients with colon cancer, who had available survival follow-up information (Table EV4). Two representative IHC images, respectively, for low and high AIF expressions of cancer tissues are shown in Fig EV5I. In this cohort, 70.73% (57/82) cancer tissues presented a higher AIF expression (AIF^{high} tumors), while 29.27% had a lower AIF expression (AIF^{low} tumors) (Fig EV5J). Intriguingly,

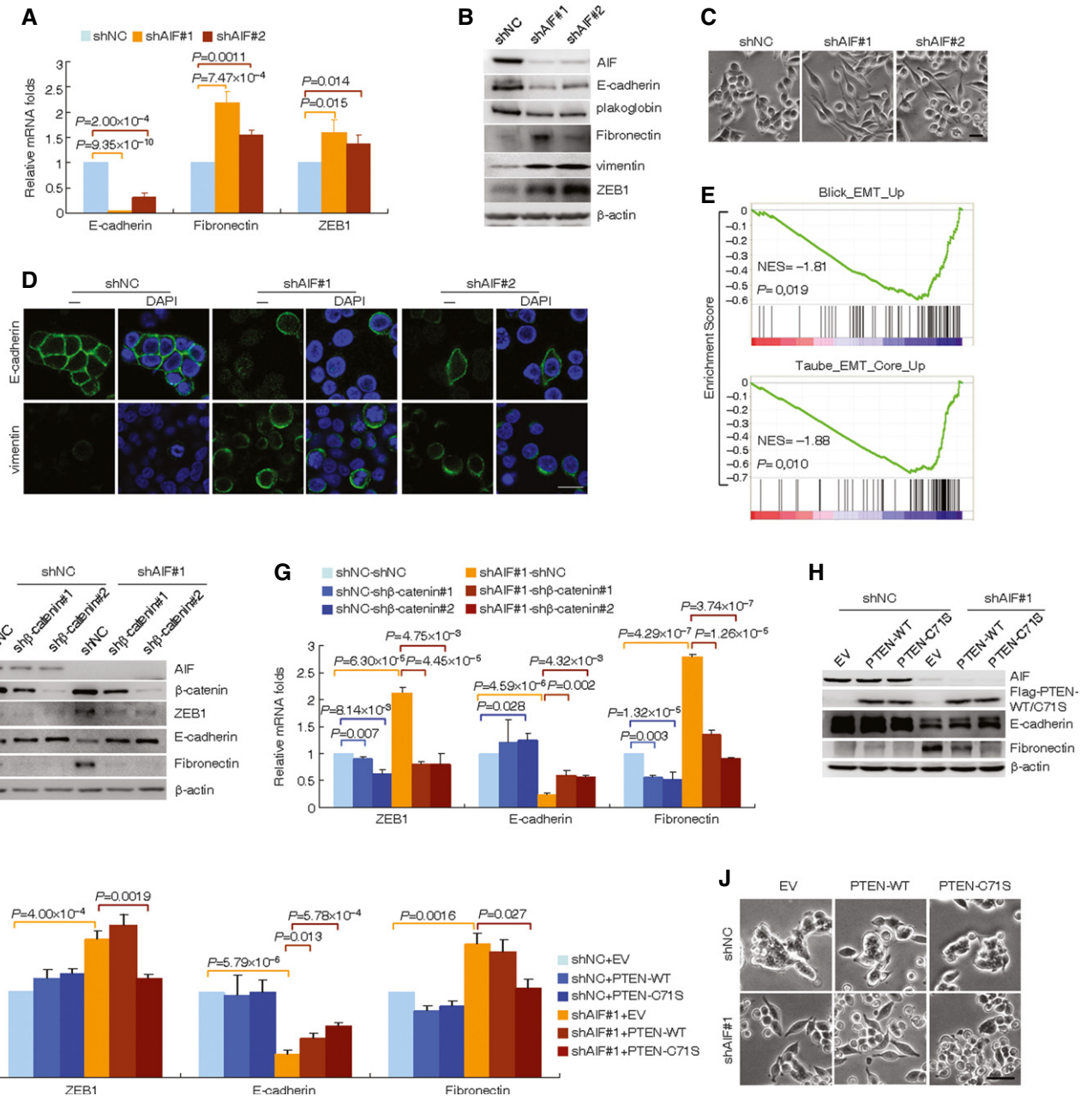

Figure 6. AIF knockdown induces the EMT program through oxidative inactivation of PTEN.

A The folds of relative mRNA levels of the indicated genes against shNC-infected cells were quantified by quantitative real-time PCR in shAIF-infected SW620 cells. Data represent means and s.d of three independent experiments. Two-sided unpaired *t*-test.

B Western blots for the indicated proteins in shNC- and shAIF-infected cells.

C The morphology of shNC- and shAIF-infected SW620 cells under phase contrast microscopy. Scale bar represents 50 μm.

D Immunofluorescence staining of E-cadherin and vimentin together with re-staining of DAPI in shNC- or shAIF-infected SW620 cells. Scale bar represents 10 μm.

E GSEA data showing the negative correlations of AIF with two published EMT gene signatures in TCGA Colon Adenocarcinoma as described in the text. *y*-axis: value of the ranking metric; *x*-axis: the rank for all genes. The graph on the bottom of each panel represents the ranked, ordered, non-redundant list of genes. Genes on the far left (red) most positively correlated with AIF, and genes on the far right (blue) most negatively correlated with AIF. On each panel, the vertical black lines indicate the position of each of the genes of the studied gene set in the ordered, non-redundant dataset. The green curve corresponds to the ES (enrichment score) curve, which is the running sum of the weighted enrichment score obtained from GSEA software. NES, normalized enrichment score.

F, G Two shRNAs against β-catenin (shβ-catenin#1 and shβ-catenin#2) along with shNC were transfected into shNC- or shAIF#1-infected SW620 cells. Western blots for the indicated proteins (F) and quantitative real-time PCR for mRNA levels of the indicated genes (G) were performed. Data represent means and s.d of three independent experiments. Two-sided unpaired *t*-test.

H–J EV, PTEN-WT, or PTEN-C71S was transfected into shNC- or shAIF#1-infected SW620 cells. Western blots for the indicated proteins (H), quantitative real-time PCR for mRNA levels of the indicated genes (I), and morphological observations under phase contrast microscopy (J, scale bar represents 50 μm) were performed. Data represent means and s.d of three independent experiments. Two-sided unpaired *t*-test.

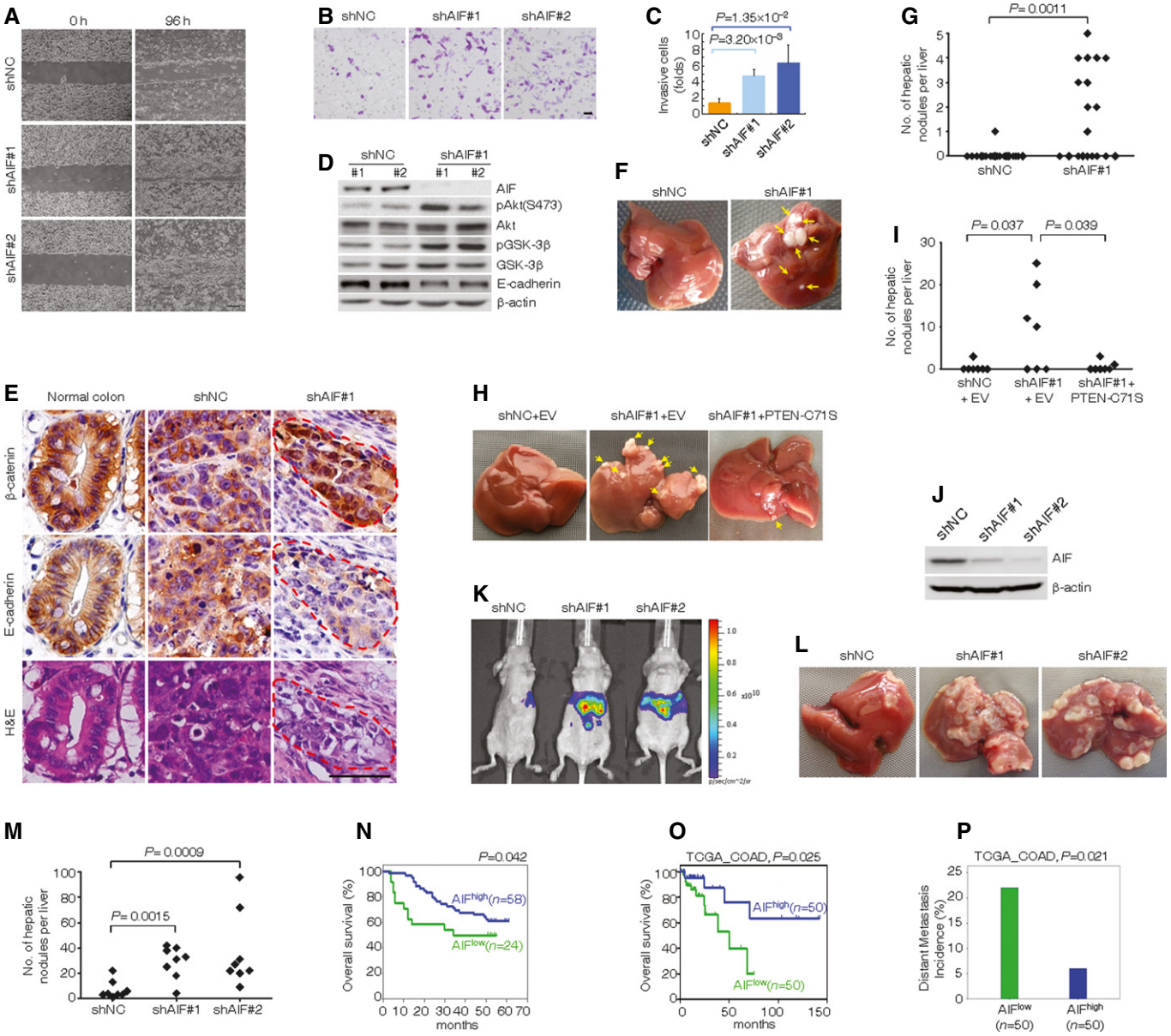

Figure 7. Low expression of AIF promotes metastasis and correlates with poor survival.

A Representative images of shNC- or shAIF-infected SW620 cells before and 96 h after wound healing under phase contrast microscopy. Scale bar represents 500 μm.

B, C Representative images of invasion assays on a Matrigel invasion chamber of shNC- and shAIF-infected SW620 cells (B) and folds of invasive shNC- or shAIF-infected SW620 cells were calculated (C). Scale bar represents 100 μm. Data represent means and s.d of three independent experiments. Two-sided unpaired *t*-test.

D, E Western blots for the indicated proteins (D) and representative images of IHC staining of β-catenin and E-cadherin (E) in colon xenografts derived from shNC- or shAIF#1-infected SW620 cells. Tumor area was marked by a dashed line. Scale bar, 50 μm.

F, G Representative macroscopic images of the livers (F) and the numbers of hepatic metastatic nodules per liver (G) from mice receiving orthotopic implantation of shNC- or shAIF#1-infected SW620 cells. The metastatic nodules were marked by yellow arrowheads. Each group with 19 mice, two-sided unpaired *t*-test.

H, I Representative macroscopic images of the livers (H) and the numbers of hepatic metastatic nodules per liver (I) for mice receiving intrasplenic injections of EV- or PTEN-C71S-expressing SW620-shNC and SW620-shAIF#1 cells. Each group with 7 mice. The metastatic nodules were marked by yellow arrowheads. Two-sided unpaired *t*-test.

J Western blots for the indicated proteins of shNC- or shAIF-infected GFP-luciferase-labeled HT29 cells.

K–M Representative BLI images (K), macroscopic images (L), and the numbers of hepatic metastatic nodules per liver (M) of mice 4 weeks after receiving intrasplenic injections of GFP-luciferase-labeled HT29 cells with or without AIF knockdown. Each group with 8 mice. Two-sided unpaired *t*-test.

N, O Kaplan–Meier estimates of overall survival of subjects with colon cancers of high and low AIF expressions in our cohort (N) and TCGA Colon Adenocarcinoma dataset (O).

P Metastasis ratios of patients, respectively, with high and low AIF expressions in TCGA Colon Adenocarcinoma dataset.

Kaplan–Meier analysis revealed that the patients with AIF-low tumors showed significantly poorer overall survival than those with AIF-high tumors (Fig 7N). We further evaluated the prognosis value of AIF expression in 375 cases of patients from TCGA Colon Adenocarcinoma with survival information and found that patients with tumors expressing the top and bottom 15% AIF mRNA levels (designated as AIF^{high} and AIF^{low}), respectively, presented favorable and poor overall survival (Fig 7O). What is more, the risk of distant metastasis for AIF^{low} patients was also much higher than that of AIF^{high} patients (Fig 7P). The positive correlation between AIF expression and overall survival could also be found in patients with breast cancer and the squamous cell lung cancer from microarray datasets TCGA Breast Invasive Carcinoma (Fig EV5K) and TCGA Lung Squamous Cell Carcinoma (Fig EV5L).

Discussion

Although the dual roles of AIF in life and death have been proposed [4], its pathological significances have few understanding. In humans, progressive mitochondrial encephalomyopathy and Cowchock syndrome are only two disorders that have been attributed to AIF so far [46,47]. However, the expression of death and survival-related functions presenting AIF and its overall significances in cancers remain largely unknown. Herein, we showed that AIF can physically interact with PTEN, for which its two FAD-binding domains and phosphatase-dependent N-terminal moiety of PTEN are, respectively, required. In accordance with this, all three short isoforms of AIF carrying an FAD-binding domain also interact with PTEN, although AIFsh3 is localized in cytoplasm. PTEN, one of the most common tumor suppressors, has phosphatase-dependent and phosphatase-independent functions, which appear to be dependent upon its localization in cytosol or nucleus [19]. It was reported that the canonical PTEN protein can packaged into exosomes and is transferred from one cell to another through vesicles [48], and PTEN-Long, a translational variant of PTEN that adds an additional 173 N-terminal amino acids to the canonical protein, is secreted and can be detected in human serum and plasma [49]. Although a mass spectrometry, GFP tagging, and machine learning-based analysis did not report PTEN in a mitochondrial compendium of 1,098 genes and their protein expression across 14 mouse tissues [23], several lines of evidence demonstrated the PTEN localization to the mitochondria [20–22], and PTEN-Long was also be shown to localize to the mitochondria besides the cytoplasm [50]. Here, we showed that PTEN is also an internal mitochondrial protein in cancer cell lines or primary freshly harvested mouse cardiac muscle cells, which were confirmed by immunoelectron microscopy and biochemical fractionation experiments. Bioinformatics analysis showed that PTEN lacks a canonical MLS sequence, resembling some MLS-lacking but still mitochondria-localizing proteins such as p53 and Stat3 [51,52]. Recently, Naguib and coworkers reported that cytoplasmic PTEN is distributed along microtubules and tethered to vesicles [53]. It remains to be investigated whether PTEN is brought into mitochondria and other compartments by such vesicles. Actually, a previous report also showed the localization of PTEN in the endoplasmic reticulum [20]. Another possibility is that AIF carries a fraction of PTEN to the mitochondria interior, which could be partially supported by the fact that AIF-interacting PTEN-N was more potently localized into mitochondria than PTEN-C (data not shown), which did not bind with AIF.

Our further investigations revealed that, as an oxidoreductase, AIF inhibits the *in vitro* oxidation of PTEN. AIF knockdown makes PTEN be oxidized, which can be rescued by re-expression of AIF or NAC treatment. Accordingly, AIF loss inactivates the phosphatase activity of PTEN, followed by the activation of Akt/GSk-3β and β-catenin signaling pathway. The cytosolic AIFsh3 also rescues AIF knockdown-induced PTEN oxidation. Of note, only a small fraction of PTEN is oxidized compared to total PTEN upon AIF knockdown. The exposure to low concentrations of H_2O_2 also induces oxidative modification of a small fraction of PTEN accompanied with the increased Akt phosphorylation. The ectopically expressed PTEN-C71S mutant, whose cysteine is essential for intracellular intramolecular disulfide bond formation of PTEN oxidation, can rescue all the AIF knockdown-induced effects. Therefore, partial modification of PTEN by oxidation contributes to the inactivation of total PTEN and thus activation of Akt. Biochemically, it appears that most documented PTEN posttranslational modifications cause a decrease in PTEN enzymatic activity *in vitro*. Therefore, we are facing the question why the oxidation of a small portion of PTEN might compromise the activity of the major pool of un-oxidized PTEN. Recently, it is reported that PTEN exerts higher phosphatase activity in homodimers. When heterodimerizing with wild-type PTEN, catalytically inactive PTEN mutants constrain the phosphatase activity of wild-type PTEN in a dominant-negative manner [54]. Thus, we speculate that the small portion of oxidized PTEN might form heterodimer with and inhibit the activity of un-oxidized PTEN. In addition, a previous report found that the peroxidase Prdx1, which catalyzes peroxide reduction to balance cellular H_2O_2 levels [55,56], interacts with and protects PTEN from oxidation-induced inactivation [11]. Txnip was also reported to be required to maintain sufficient thioredoxin NADPH activity to reductively reactivate oxidized PTEN and oppose Akt downstream signaling in non-lipogenic tissues [12]. It deserves to be further explored whether AIF, Prdx1, and/or Txnip are either independent or combined with each other to be implicated in control of PTEN activity by reversible oxidation.

Tumorigenesis and metastasis are caused by the dysregulation of a series of intracellular signals such as WNT signaling, which has been well established as a metastasis regulator of cancer. The canonical WNT/β-catenin signaling pathway functions by stabilizing β-catenin, whose phosphorylation by GSK-3β results in degradation through the ubiquitin–proteasome pathway. The stabilized β-catenin is allowed to translocate into the nuclei where it transcriptionally activates the WNT/β-catenin target genes. Intriguingly, there is a clear inverse correlation between AIF and WNT/β-catenin signaling target genes in several independent microarray datasets from different types of cancers. In line with this, knockdown of AIF significantly increases transcriptional activity of WNT/β-catenin signaling and expressions of WNT/β-catenin target genes. In particular, β-catenin knockdown almost completely blocked AIF silencing-induced phenotype. These data support the role of activated β-catenin in AIF knockdown-induced effects.

Inactivation of GSK-3β leads to the nuclear accumulation of β-catenin, which in turn activates the WNT/β-catenin signaling pathway and promotes the expression of a bunch of WNT/β-catenin target genes. Although a previous report proposed that cross talk

between the PI3K and WNT/β-catenin pathways might be prohibited and WNT/β-catenin-mediated transcriptional activity was not modulated by the activation of the PI3K/Akt pathway [31], our results showed that the oxidation-resistant mutant of PTEN, PTEN-C71S, but not wild-type PTEN, as well as PI3K/Akt inhibitor and NAC treatment, reversed AIF knockdown-induced expressions of WNT/β-catenin signaling target genes, supporting that AIF regulates β-catenin signaling through PTEN-PI3K/Akt pathway.

There has been a clear connection between WNT/β-catenin signaling activation and metastasis [42,57,58]. Indeed, AIF silencing induces EMT and increases the *in vitro* mobility and invasiveness, and promotes *in vivo* hepatic metastasis of orthotopically implanted tumors in nude mice. In line with this, AIF expression level is positively correlated with overall survival in our cohort of colon cancer patients, which can also be found in several microarray datasets for colon, breast, and lung cancers. Notably, the fact that β-catenin knockdown almost completely reversed the increase in ZEB1 protein and EMT program upon AIF silencing, further supporting β-catenin dependency of the observed phenotypic changes in response to AIF depletion. It should be pointed out that a previous report, which showed that human colon carcinoma cell lines with AIF knockout by homologous recombination failed to form tumors in athymic mice or grow in soft agar [59], was completely inconsistent with our results from cancer cells with AIF knockdown. We extrapolated that the reasons to cause the apparent discrepancy might due to different levels of AIF loss in two different assays because AIF presents dual roles in cell death and survival. Also, two previous reports showed that there was higher AIF expression in the majority of gastric carcinoma [60] and colorectal carcinoma [61]. The similar phenomena could also been found in our colorectal carcinoma cohort, although AIF expression was shown to be decreased in many other tumor types, contributing to their chemoresistance [2,62]. Our unpublished data showed that hypoxia inhibits AIF expression, and low AIF expression mainly exists in hypoxic regions of cancer tissues, although most cancer tissues expressed higher AIF. As a multifunctional protein, we proposed that its pro-survival function in cancer cells with high AIF expression contributes to tumorigenesis, and its role as antagonist of PI3K signaling in cancer cells with low AIF expression during hypoxic environment is correlated with EMT and metastasis of cancers.

Totally, our results provide evidence for an essential role of AIF in controlling tumor invasion and metastasis, and novel mechanism of protecting PTEN from oxidation, although the functional interaction between PTEN and AIF in mitochondria and/or elsewhere needs to further addressed. Our findings would shed new sights for understanding the mechanisms of cancer metastasis and exploring new potential antimetastasis therapy.

Materials and Methods

Cell culture and transfections

SW620, SW480, and LNCaP cells were maintained in RPMI-1640 supplemented with 10% FBS. DU145 and 293T cells were maintained in DMEM supplemented with 10% FBS. PC3 cells were maintained in F-12K supplemented with 10% FBS. HT29 cells were maintained in McCoy's 5A supplemented with 10% FBS. Cells are cultured in a humidified incubator at 37°C with 5% CO_2. For transient transfection, Lipofectamine 2000 transfection reagent (Invitrogen, Carlsbad, CA) was used following the manufacturer's protocol. For cell transduction, retroviruses or lentiviruses were prepared by transient cotransfection with helper plasmids into 293T cells using FuGENE 9 (Roche, Basel, Switzerland).

Antibodies

Antibodies against AIF-FL (#4642), β-catenin (#9587), Akt (#9272), pAkt (#4060), GSK-3β (#9315), pGSK-3β (#9331), PTEN (#9559), Cox-IV (#4850), and His (#2366) were purchased from Cell Signaling Technology (Danvers, MA); the antibody for AIFsh2 and AIFsh3 (LS-C147989) from Lifespan Biosciences (Seattle, WA); Streptavidin–HRP Conjugate (89880D) from Thermo Fisher Scientific (Waltham, MA); Ndufs1 (12444-1-AP) and Ndufs3 (15066-1-AP) from Proteintech Group (Chicago IL); HA (sc-805) and LaminB (sc-6216) from Santa Cruz; GST (013-21851) from Wako; Flag (A8592) and β-actin (A5316) from Sigma-Aldrich.

Plasmids and shRNAs

Mito-PTEN was generated by inserting PTEN coding sequence (CDS) into the pCMV/*myc*/mito vector purchased from Invitrogen, Life Technologies. The coding sequence for mitochondrial targeting sequence used here is shown as follows: ATG TCC GTC CTG ACG CCG CTG CTG CTG CGG GGC TTG ACA GGC TCG GCC CGG CGG CTC CCA GTG CCG CGC GCC AAC ATC CAT CGT TTG. Plasmid expressing Flag-tagged AIF was generated by inserting AIF CDS into pCI-Flag vector. Plasmids expressing 3× Flag-tagged PTEN, PTEN-N, and PTEN-C and AIFsh, AIFsh2, and AIFsh3 were generated by inserting correspondent CDS into pBabe-3× Flag vector. Plasmids expressing untagged AIF and PTEN were generated by inserting correspondent CDS into pMSCVpuro and pQCXIN vectors, respectively. For HA-tagged PTEN, PTEN CDS was cloned and inserted into pHACB vector. Plasmid expressing His-tagged PTEN were generated by inserting PTEN CDS into pET-28a (+) vector. Plasmids expressing GST-tagged AIF and its mutants were generated by inserting correspondent CDS into pEGX-5X-1 vector. Plasmids for knockdown were constructed by inserting corresponding shRNA sequences into the pSIREN Retro-Q plasmid (clontech). The shRNA sequences specially targeting AIF, PTEN, and β-catenin are, respectively, TAGCGGTCGCCGAAATGTT (shAIF#1), CTGGTATCCGATC AGAGAG (shAIF#2), CGGGAAGACAAGTTCATGTACTT (shPTEN), CCATTGTTTGTGCAGCTGCTT (shβ-catenin#1), and GCTTGGAA TGAGACTGCTGAT (shβ-catenin#2).

Immunoprecipitation

Cells were harvested and lysed with immunoprecipitation buffer (50 mM Tris–HCl, pH 7.6; 150 mM NaCl; 1 mM EDTA; 1% NP-40; 1 mM DOC; 1% protease inhibitor cocktail; 1 mM PMSF). After brief sonication, the lysates were centrifuged at 12,000 *g* for 10 min at 4°C. For immunoprecipitation of Flag-tagged proteins, supernatants were incubated with anti-Flag M2 Affinity Gel (Sigma-Aldrich) at 4°C overnight. Otherwise, supernatants were incubated with indicated antibodies overnight and protein A/G-agarose beads (Santa Cruz, CA) for 4 h at 4°C. The precipitates were washed three

times with immunoprecipitation buffer, boiled in sample buffer, and subjected to immunoblot assay.

Nano-LC–ESI–MS/MS analysis

Immunoprecipitation samples were separated by SDS–PAGE and visualized with colloidal Coomassie blue. The lane from gels was cut into 1-mm slices, and each slice was washed twice with 50 mM NH_4HCO_3 and 50% ACN and dehydrated with acetonitrile (ACN). Proteins were reduced and alkylated by treating them with 10 mM DTT and 55 mM iodoacetamide, respectively. After washing with 50 mM NH_4HCO_3 and ACN, proteins were digested in gel with trypsin (Promega, Madison, WI) and incubated overnight at 37°C. Tryptic peptides were extracted from the gel pieces with 60% ACN and 0.1% trifluoroacetic acid. The peptide extracts were vacuum-centrifuged to dryness. Dried peptides were dissolved in 10 μl of 2% ACN and 0.1% trifluoroacetic acid. Samples were desalted and preconcentrated through a Michrom peptide CapTrap (MW 0.5–50 kDa, 0.5 × 2 mm; Michrom BioResources, Inc., Auburn, CA). The eluent was vacuum-centrifuged to dryness and then reconstituted in 2% ACN and 0.1% formic acid.

For LC–MS/MS analysis, 10 μl samples were introduced from an autosampler (HTS-PAL, CTC Analytics, Zwingen, Switzerland) at a flow of 1 μl/min for 15 min onto a reverse-phase microcapillary column (0.1 × 150 mm, packed with 5 μm 100 Å Magic C18 resin; Michrom Bioresources) using a HPLC (Paragram MS4, Michrom Bioresources). The reverse-phase separation of peptides was performed at a flow of 0.5 μl/min using the following buffers: 2% ACN with 0.1% formic acid (buffer A) and 98% ACN with 0.1% formic acid (buffer B) using a 90-min gradient (0–35% B for 90 min, 80% B for 8 min, 95% B for 12 min, and 0% B for 20 min). The eluate was introduced directly onto a hybrid linear ion trap (LTQ) Orbitrap mass spectrometer (ThermoFinnigan, San Jose, CA, USA) equipped with ADVANCE Spray Source (Michrom Bioresources). A high-resolution MS survey scan was obtained for the m/z 350–1,800, R = 100,000 (at m/z 400) and ion accumulation to a target value of 10^6. Siloxane (m/z 445.120025) was used as an internal standard. MS/MS spectra were acquired using data-dependent scan from the ten most-intense ions with charge states ≥ 2 in the survey scan (as determined by the Xcalibur mass spectrometer software in real time). Only MS signals exceeding 500 ion counts triggered a MS/MS attempt, and 5,000 ions were acquired for a MS/MS scan. Dynamic mass exclusion windows of 27 s were used. Singly charged ions and ions with unassigned charge states were excluded from triggering MS/MS scans. The normalized collision energy was set to 35%. Tandem mass spectra were extracted with Xcalibur version 2.0.7. The MS/MS data were searched against The International Protein Index (IPI) human database (ipi.HUMAN.v3.73 downloaded from ftp.ebi.ac.uk/pub/databases/IPI) containing 179304 entries using SORCERERSEQUEST (Bioworks version 3.5, ThermoFinnigan), which was run on the Sage-N Sorcerer2 (Thermo Electron, San Jose, CA). Peptide (parent ion) tolerance of 10 ppm, fragment ion tolerance of 1 Da, and 3 missed cleavages were allowed, and fixed modification of carbamidomethylation on Cys (157 Da) and differential modification of oxidation on Met (16 Da) were used. The XCorr scores cutoffs for each charge state were as follows: 2.5 (+2), 3.0 (+3), 3.5 (+4). The results were further analyzed by Scaffold 3 proteome software (Portland, OR), which integrates both Protein Prophet and Peptide Prophet. Two unique peptides must be identified independently for each protein, the peptide probability must be 95% or higher, and the protein probability must be 95% or higher.

Density-based fractionation

Density-based fractionation was performed with the Edge 200 Separation System from Prospect Biosystem, LLC (Newark, NJ), according to the manufacturer's instructions. Briefly, 2×10^8 SW620 cells were resuspended in homogenizing buffer (HB, 10 mM Tris–HCl pH 6.7, 150 mM $MgCl_2$, 10 mM KCl) supplemented with 1% protease inhibitor cocktail and 1 mM PMSF, and homogenized with 20 strokes at 4°C. The homogenate was transferred to centrifuge tubes and centrifuged at 1,000 *g* for 10 min to remove the nucleus. The supernatant, which is post-nuclear supernatant (PNS), was collected and centrifuged at 10,000 *g* for 5 min at 4°C. The supernatant was discarded, and the first density extraction medium (8.5% w/w sucrose) was added into the tube to resuspend the pellet which contained almost all of the subcellular particles. The suspension was centrifuged at 10,000 *g* for 5 min at 4°C, and the supernatant was collected as the first fraction. These same steps were continued using serially increasing sucrose density extraction medium: 10, 15, 20, 25, 30, 35, 40, 45, 50, 55 and 60%. A total of 12 fractions were obtained.

Subcellular cell fractionation, mitochondria purification, and proteolysis protection assay

Cells were separated into different fractions according to methods described previously [63,64]. Briefly, cells were harvested and rinsed with mitochondria isolation buffer (MIB, 0.25 M sucrose and 10 mM Tris–HCl, pH 7.4). Then, cells were resuspended in MIB supplemented with 1% protease inhibitor cocktail and homogenized using a glass Dounce homogenizer (Kontes, Sigma-Aldrich) with 20 strokes at 4°C. The homogenate was centrifuged at 1,000 *g* for 10 min to pellet the nucleus. The supernatant was then centrifuged at 15,000 *g* for 20 min at 4°C to pellet the raw mitochondria. Cytoplasmic proteins in the post-mitochondria supernatant were precipitated with chloroform and methanol according to Klotz's methods [65]. To further enrich mitochondria, the pellet of raw mitochondria was resuspended in 36% iodixanol (Sigma-Aldrich) and overlaid with 30 and 10% iodixanol. The gradient was ultracentrifuged (80,000 *g*, 3 h) at 4°C, and the purified mitochondria were collected at the interface between 10% and 30% iodixanol and washed twice with MIB. Samples of each fraction were prepared by adding sample buffer and subjected to immunoblot analysis.

Equal aliquots of purified mitochondria pellet resuspended in MIB were incubated at 37°C without protease inhibitors in the presence of 0.25 μg/μl trypsin and 1% Triton X-100 alone or in combination for 10 min. After the addition of sample buffer, proteolysis protection reactions were then subjected to immunoblot analysis as indicated.

RT–PCR and quantitative real-time PCR

Total RNA was prepared using TRIzol (Invitrogen) following the manufacturer's instructions. A total of 2 μg RNA was subjected to

reverse transcription to synthesize cDNA using M-MLV Reverse Transcriptase (Promega, Fitchburg, WI). RT–PCR primers for detection of AIFsh, AIFsh2, and AIFsh3 were designed according to a previous report [17]. Quantitative real-time PCR was performed using the SYBR Green PCR Master Mix (Applied Biosystems, Foster City, CA). Paired primers were used as follows.

Primers for quantitative real-time PCR

Genes	Forward primers	Reverse primers
DKK1	GAGTACTGCGCTAGTCCCAC	TGGAATACCCATCCAAGGTGC
ID2	AGGAAAAACAGCCTGTCGGA	TGGTGATGCAGGCTGACAAT
AXIN2	GAGAGTGAGCGGCAGAGC	CGGCTGACTCGTTCTCCT
LEF1	TCCTGAAATCCCCACCTTCT	TGGGATAAACAGGCTGACCT
TCF4	CATGCCACCAGGACTACAGG	TTCTCACGCTCTGCCTTCTG
MMP7	GGCTTTAAACATGTGGGGCA	GACTGCTACCATCCGTCCAG
ACTIN	CATCCTCACCCTGAAGTACCC	AGCCTGGATAGCAAC GTACATG

Patients and IHC

Formalin-fixed and paraffin-embedded tumor specimens from colon cancer patients were purchased from Shanghai Outdo Biotech Co (Shanghai, China). Tissue slides were de-paraffinized at 60°C, followed by treatment with xylene and a graded alcohol series. The endogenous peroxidase activity was blocked by incubation in a 3% hydrogen peroxide solution for 15 min. Antigen retrieval was carried out by immersing the slides in 10 mM sodium citrate buffer (PH 6.0) and maintained at a sub-boiling temperature for 10 min. The slides were rinsed in PBS and incubated with 5% BSA to block no-specific staining. Then, the slides were incubated with the primary antibody overnight at 4°C in a humid chamber. On the next day, the slides were visualized by standard avidin-biotinylated peroxidase complex method. Finally, hematoxylin was used for counterstaining.

All of the staining was assessed by pathologists blinded to the origination of the samples and subject outcome. Each specimen was assigned a score according to the intensity of the nucleus, cytoplasmic, and/or membrane staining (no staining = 0; weak staining = 1, moderate staining = 2, strong staining = 3) and the area extent of stained cells (0% = 0, 1–24% = 1, 25–49% = 2, 50–74% = 3, 75–100% = 4). The final immunoreactive score (IRS) was determined by multiplying the intensity score with the extent score of stained cells, ranging from 0 (the minimum score) to 12 (the maximum score). Scores ≤ 4 and scores > 4 were considered as low and high AIF expression, respectively. Detailed information of the two cohorts is shown in Tables EV3 and EV4.

GST pull-down assay

We expressed and purified GST and GST fusion proteins as previously described [66]. His-tagged PTEN was purified as previously described [55]. Ten microgram His-tagged PTEN or the 293T extracts expressing Flag-tagged PTEN-N were mixed with 10 μg of GST derivatives bound to glutathione–Sepharose beads in 0.5 ml of binding buffer. The binding reaction was performed overnight at 4°C, and the beads were subsequently washed three times with the binding buffer.

Electron microscopy

Whole cells or isolated mitochondria were fixed in 2% formaldehyde and 0.2% glutaraldehyde (EM grade) for 12 h at 4°C, incubated in 0.1 M glycine for 10 min at 22°C to remove free aldehydes, dehydrated through a gradual series of ethanol to 100%, and transferred into a mixture of 50:50 (v/v) resin (Lowicryl K4M):100% acetone for 2 h at 22°C. Samples were transferred to aliquots of fresh resin (×3) and applied to filling embedding capsules for 48 h at 60°C. Ultrathin sections were cut using an ultramicrotome (Reichert-Jung Ultracut E), placed on nickel support rids, blocked in 4% BSA for 1 h at 22°C, and incubated with an antibody to PTEN or control non-binding IgG. After the addition of gold-conjugated secondary antibodies (1:40, TED PELLA), samples were washed, exposed to OsO_4 vapor for 1 h at 22°C, post-stained with uranyl acetate and lead citrate, and analyzed on a Philips EM10 electron microscope at 80 kV.

Western blots

Cells were rinsed with ice-cold 1× PBS and lysed in non-reducing buffer containing 100 mM Tris–HCl, pH 6.8, 2% SDS, 50 mM IAA, supplemented with PMSF and cocktail, or reducing buffer containing additional 100 mM DTT. Cell lysates were separated by 8–12.5% SDS–polyacrylamide gel, transferred to nitrocellulose membrane (Bio-Rad, Richmond, CA), blocked by 5% nonfat milk in TBS, and immunoblotted with the indicated antibodies. Followed by incubation with horseradish peroxidase (HRP)-linked second antibody (Cell signaling, Beverly, MA) at room temperature, detection was performed by SuperSignal West Pico Chemiluminescent Substrate Kit (Pierce, Rockford, IL) according to the manufacturer's instructions.

Recombinant expression, *in vitro* incubation, and DCP-Bio1 labeling

Recombinant full-length PTEN, AIF, and its mutants were expressed in *E. coli* using the SUMO-fusion expression system (Life Sensor, Tokyo, JP) and purified by nickel chelating, ion exchange, and gel filtration columns as reported [67]. Recombinant proteins were kept in 50 mM Tris–HCl, pH 7.8. Incubation reaction was carried out by incubating PTEN and AIF alone or together in the presence of 200 μM NADH (Sigma-Aldrich) and protease inhibitors PMSF and cocktail at 4°C for 1 h. Afterward, the mixtures were prepared under reducing or non-reducing condition and analyzed with Western blots. For DCP-Bio1 (KeraFAST, Boston, MA) labeling, the mixtures were incubated with 500 μM DCP-Bio1 in the presence of 50 mM IAA at 4°C for additionally 1 h. Finally, the mixtures were prepared under reducing condition and analyzed with Western blots.

PTEN phosphatase activity assay

For endogenous PTEN phosphatase activity, SW620 cells with or without AIF knockdown were lysed in phosphatase inhibitors-free lysis buffer. PTEN proteins were immunoprecipitated from lysates

with anti-PTEN antibody. Immunoprecipitates were then washed twice, followed by a final wash in PTEN enzyme reaction buffer (10 mM Hepes, 150 mM NaCl, 10 mM DTT pH 7.2). For recombinant PTEN phosphatase activity, recombinant PTEN was incubated with or without AIF. Then, the phosphatase reactions were done following the manufacturer's instructions (Echelon Biosciences) and a previous study. Briefly, the immunoprecipitated PTEN proteins or *in vitro* reactions were incubated with PTEN enzyme reaction buffer for an appropriate amount of time at 37°C in a 96-well plate coated with $PI(3,4,5)P_3$. After the removal of PTEN proteins from plates, $PI(4,5)P_2$ was determined according to the manufacturer's instructions. Absorbance was measured at 450 nm in a microplate reader, and $PI(4,5)P_2$ produced was calculated from a standard curve.

Immunofluorescence

Coverslip-grown cells were fixed in 4% paraformaldehyde for 15 min at room temperature and rinsed three times in PBS. Coverslips were permeabilized in 0.3% Triton X-100/PBS for 15 min and rinsed three times in PBS. Then, coverslips were blocked in 2% BSA/PBS for 1 h at room temperature. Primary antibodies were applied at 1:100 dilution in staining buffer overnight at 4°C in a humid chamber. Coverslips were subsequently washed three times. Secondary antibodies (Alexa Fluor secondary 488, 595; Invitrogen) were applied at 1:200 dilution in staining buffer for 1 h at 37°C in a humid chamber in the dark. Prior to mounting with Vectorshield with DAPI (Vector Laboratories, CA), coverslips were washed three times more in PBS. Immunofluorescence analysis was conducted on a Carl Zeiss LSM710 Laser Scanning Microscope.

Dual luciferase reporter assay

Luciferase activity was measured using the Dual-Luciferase Reporter Assay System (Promega). Cells at 50% confluence in 12-well plates were transfected using Lipofectamine 2000 (Invitrogen). Topflash/Fopflash luciferase reporter plasmid kit was purchased from Upstate, Millipore. All experiments were performed in triplicate. Expressions of firefly and *Renilla* luciferases were analyzed 36 h after transfection according to the manufacturer's instructions.

Microarray datasets

Expression data of the TCGA Colon Adenocarcinoma, TCGA Breast Invasive Carcinoma, and TCGA Lung Squamous Cell Carcinoma datasets are RSEM Z-scored values and downloaded from http://gdac.broadinstitute.org. Grasso Prostate dataset was downloaded from Gene Expression Omnibus (GEO).

Animal experiments

Animal care and experiments were performed in strict accordance with the "Guide for the Care and Use of Laboratory Animals" and the "Principles for the Utilization and Care of Vertebrate Animals" and were approved by the committee for humane treatment of animals at Shanghai Jiao Tong University School of Medicine. We inoculated shNC and shAIF-1 SW620 cells (5×10^6 each mouse) subcutaneously into nude mice (Shanghai Laboratory of Animal Center, Chinese Academy of Sciences), and tumor volume was monitored every 2 days. One mouse from each group was sacrificed at day 15, and tumors were harvested and cut into pieces in PBS. Orthotopic implantation of the subcutaneous engraftment was performed by suturing tumor mass (approximately 2 mm in diameter) on the cecum wall. For intrasplenic injection, cells (3×10^6 each mouse) were injected into the spleen of nude mice.

Statistical analyses

All *in vitro* experiments were repeated at least three times. We defined overall survival as the time from the date of diagnosis to the subject's death from colon cancer. Patients who were alive at the last follow-up were censored at the last follow-up. Survival curves were derived from Kaplan–Meier estimates, and we compared the curves using log-rank test. Unless described, the *P*-values for comparison between groups were obtained by Student's *t*-test. All statistical tests were two-sided, and P-value < 0.05 was considered to be statistically significant.

Expanded View for this article is available online:
http://embor.embopress.org

Acknowledgements
This work was supported by National Key Research Program of China (NO2015CB910403), National Natural Science Foundation (81230048; 81430061; 81502001).

Author contributions
S-MS and MG performed most of the experiments and data analysis. ZX, F-FZ, and YY contributed to partial cellular experiments and plasmid construction. X-YZ helped to analyze dataset, and G-QC supervised the project, designed experiments, analyzed results, and wrote the paper.

Conflict of interest
The authors declare that they have no conflict of interest.

References

1. Susin SA, Lorenzo HK, Zamzami N, Marzo I, Snow BE, Brothers GM, Mangion J, Jacotot E, Costantini P, Loeffler M *et al* (1999) Molecular characterization of mitochondrial apoptosis-inducing factor. *Nature* 397: 441 – 446
2. Sevrioukova IF (2011) Apoptosis-inducing factor: structure, function, and redox regulation. *Antioxid Redox Signal* 14: 2545 – 2579
3. Joza N, Pospisilik JA, Hangen E, Hanada T, Modjtahedi N, Penninger JM, Kroemer G (2009) AIF: not just an apoptosis-inducing factor. *Ann N Y Acad Sci* 1171: 2 – 11
4. Hangen E, Blomgren K, Benit P, Kroemer G, Modjtahedi N (2010) Life with or without AIF. *Trends Biochem Sci* 35: 278 – 287
5. Lendahl U, Lee KL, Yang H, Poellinger L (2009) Generating specificity and diversity in the transcriptional response to hypoxia. *Nat Rev Genet* 10: 821 – 832
6. Hanahan D, Weinberg RA (2011) Hallmarks of cancer: the next generation. *Cell* 144: 646 – 674
7. Leslie NR, Yang X, Downes CP, Weijer CJ (2007) PtdIns(3,4,5)P(3)-dependent and -independent roles for PTEN in the control of cell migration. *Curr Biol* 17: 115 – 125

8. Yu CX, Li S, Whorton AR (2005) Redox regulation of PTEN by S-nitrosothiols. *Mol Pharmacol* 68: 847 – 854
9. Lee SR, Yang KS, Kwon J, Lee C, Jeong W, Rhee SG (2002) Reversible inactivation of the tumor suppressor PTEN by H_2O_2. *J Biol Chem* 277: 20336 – 20342
10. Wu Y, Zhou H, Wu K, Lee S, Li R, Liu X (2014) PTEN phosphorylation and nuclear export mediate free fatty acid-induced oxidative stress. *Antioxid Redox Signal* 20: 1382 – 1395
11. Cao J, Schulte J, Knight A, Leslie NR, Zagozdzon A, Bronson R, Manevich Y, Beeson C, Neumann CA (2009) Prdx1 inhibits tumorigenesis via regulating PTEN/AKT activity. *EMBO J* 28: 1505 – 1517
12. Hui ST, Andres AM, Miller AK, Spann NJ, Potter DW, Post NM, Chen AZ, Sachithanantham S, Jung DY, Kim JK *et al* (2008) Txnip balances metabolic and growth signaling via PTEN disulfide reduction. *Proc Natl Acad Sci USA* 105: 3921 – 3926
13. Wilkinson JC, Wilkinson AS, Galban S, Csomos RA, Duckett CS (2008) Apoptosis-inducing factor is a target for ubiquitination through interaction with XIAP. *Mol Cell Biol* 28: 237 – 247
14. Oh KH, Yang SW, Park JM, Seol JH, Iemura S, Natsume T, Murata S, Tanaka K, Jeon YJ, Chung CH (2011) Control of AIF-mediated cell death by antagonistic functions of CHIP ubiquitin E3 ligase and USP2 deubiquitinating enzyme. *Cell Death Differ* 18: 1326 – 1336
15. Zanna C, Ghelli A, Porcelli AM, Karbowski M, Youle RJ, Schimpf S, Wissinger B, Pinti M, Cossarizza A, Vidoni S *et al* (2008) OPA1 mutations associated with dominant optic atrophy impair oxidative phosphorylation and mitochondrial fusion. *Brain* 131: 352 – 367
16. Hangen E, Feraud O, Lachkar S, Mou H, Doti N, Fimia GM, Lam NV, Zhu C, Godin I, Muller K *et al* (2015) Interaction between AIF and CHCHD4 regulates respiratory chain biogenesis. *Mol Cell* 58: 1001 – 1014
17. Delettre C, Yuste VJ, Moubarak RS, Bras M, Robert N, Susin SA (2006) Identification and characterization of AIFsh2, a mitochondrial apoptosis-inducing factor (AIF) isoform with NADH oxidase activity. *J Biol Chem* 281: 18507 – 18518
18. Delettre C, Yuste VJ, Moubarak RS, Bras M, Lesbordes-Brion JC, Petres S, Bellalou J, Susin SA (2006) AIFsh, a novel apoptosis-inducing factor (AIF) pro-apoptotic isoform with potential pathological relevance in human cancer. *J Biol Chem* 281: 6413 – 6427
19. Salmena L, Carracedo A, Pandolfi PP (2008) Tenets of PTEN tumor suppression. *Cell* 133: 403 – 414
20. Bononi A, Bonora M, Marchi S, Missiroli S, Poletti F, Giorgi C, Pandolfi PP, Pinton P (2013) Identification of PTEN at the ER and MAMs and its regulation of Ca^{2+} signaling and apoptosis in a protein phosphatase-dependent manner. *Cell Death Differ* 20: 1631 – 1643
21. Zhu Y, Hoell P, Ahlemeyer B, Krieglstein J (2006) PTEN: a crucial mediator of mitochondria-dependent apoptosis. *Apoptosis* 11: 197 – 207
22. Zu L, Zheng X, Wang B, Parajuli N, Steenbergen C, Becker LC, Cai ZP (2011) Ischemic preconditioning attenuates mitochondrial localization of PTEN induced by ischemia-reperfusion. *Am J Physiol Heart Circ Physiol* 300: H2177 – H2186
23. Pagliarini DJ, Calvo SE, Chang B, Sheth SA, Vafai SB, Ong SE, Walford GA, Sugiana C, Boneh A, Chen WK *et al* (2008) A mitochondrial protein compendium elucidates complex I disease biology. *Cell* 134: 112 – 123
24. Trachootham D, Alexandre J, Huang P (2009) Targeting cancer cells by ROS-mediated mechanisms: a radical therapeutic approach? *Nat Rev Drug Discov* 8: 579 – 591
25. Harris IS, Treloar AE, Inoue S, Sasaki M, Gorrini C, Lee KC, Yung KY, Brenner D, Knobbe-Thomsen CB, Cox MA *et al* (2015) Glutathione and thioredoxin antioxidant pathways synergize to drive cancer initiation and progression. *Cancer Cell* 27: 211 – 222
26. Tsai JH, Donaher JL, Murphy DA, Chau S, Yang J (2012) Spatiotemporal regulation of epithelial-mesenchymal transition is essential for squamous cell carcinoma metastasis. *Cancer Cell* 22: 725 – 736
27. Vahsen N, Cande C, Briere JJ, Benit P, Joza N, Larochette N, Mastroberardino PG, Pequignot MO, Casares N, Lazar V *et al* (2004) AIF deficiency compromises oxidative phosphorylation. *EMBO J* 23: 4679 – 4689
28. Maehama T, Dixon JE (1998) The tumor suppressor, PTEN/MMAC1, dephosphorylates the lipid second messenger, phosphatidylinositol 3,4,5-trisphosphate. *J Biol Chem* 273: 13375 – 13378
29. Myers MP, Pass I, Batty IH, Van der Kaay J, Stolarov JP, Hemmings BA, Wigler MH, Downes CP, Tonks NK (1998) The lipid phosphatase activity of PTEN is critical for its tumor suppressor function. *Proc Natl Acad Sci USA* 95: 13513 – 13518
30. Greiner R, Palinkas Z, Basell K, Becher D, Antelmann H, Nagy P, Dick TP (2013) Polysulfides link H2S to protein thiol oxidation. *Antioxid Redox Signal* 19: 1749 – 1765
31. Ng SS, Mahmoudi T, Danenberg E, Bejaoui I, de Lau W, Korswagen HC, Schutte M, Clevers H (2009) Phosphatidylinositol 3-kinase signaling does not activate the wnt cascade. *J Biol Chem* 284: 35308 – 35313
32. Nelson WJ, Nusse R (2004) Convergence of Wnt, beta-catenin, and cadherin pathways. *Science* 303: 1483 – 1487
33. Schuijers J, Mokry M, Hatzis P, Cuppen E, Clevers H (2014) Wnt-induced transcriptional activation is exclusively mediated by TCF/LEF. *EMBO J* 33: 146 – 156
34. Hughes TA, Brady HJ (2005) Cross-talk between pRb/E2F and Wnt/beta-catenin pathways: E2F1 induces axin2 leading to repression of Wnt signalling and to increased cell death. *Exp Cell Res* 303: 32 – 46
35. Morris EJ, Ji JY, Yang F, Di Stefano L, Herr A, Moon NS, Kwon EJ, Haigis KM, Naar AM, Dyson NJ (2008) E2F1 represses beta-catenin transcription and is antagonized by both pRB and CDK8. *Nature* 455: 552 – 556
36. Grasso CS, Wu YM, Robinson DR, Cao X, Dhanasekaran SM, Khan AP, Quist MJ, Jing X, Lonigro RJ, Brenner JC *et al* (2012) The mutational landscape of lethal castration-resistant prostate cancer. *Nature* 487: 239 – 243
37. Buck E, Eyzaguirre A, Barr S, Thompson S, Sennello R, Young D, Iwata KK, Gibson NW, Cagnoni P, Haley JD (2007) Loss of homotypic cell adhesion by epithelial-mesenchymal transition or mutation limits sensitivity to epidermal growth factor receptor inhibition. *Mol Cancer Ther* 6: 532 – 541
38. Blick T, Hugo H, Widodo E, Waltham M, Pinto C, Mani SA, Weinberg RA, Neve RM, Lenburg ME, Thompson EW (2010) Epithelial mesenchymal transition traits in human breast cancer cell lines parallel the $CD44^{hi}/CD24^{lo/-}$ stem cell phenotype in human breast cancer. *J Mammary Gland Biol Neoplasia* 15: 235 – 252
39. Taube JH, Herschkowitz JI, Komurov K, Zhou AY, Gupta S, Yang J, Hartwell K, Onder TT, Gupta PB, Evans KW *et al* (2010) Core epithelial-to-mesenchymal transition interactome gene-expression signature is associated with claudin-low and metaplastic breast cancer subtypes. *Proc Natl Acad Sci USA* 107: 15449 – 15454
40. Kim H, Verhaak RG (2015) Transcriptional mimicry by tumor-associated stroma. *Nat Genet* 47: 307 – 309
41. Sanchez-Tillo E, de Barrios O, Siles L, Cuatrecasas M, Castells A, Postigo A (2011) beta-catenin/TCF4 complex induces the epithelial-to-mesenchymal transition (EMT)-activator ZEB1 to regulate tumor invasiveness. *Proc Natl Acad Sci USA* 108: 19204 – 19209

42. Nguyen DX, Chiang AC, Zhang XH, Kim JY, Kris MG, Ladanyi M, Gerald WL, Massague J (2009) WNT/TCF signaling through LEF1 and HOXB9 mediates lung adenocarcinoma metastasis. *Cell* 138: 51 – 62
43. Shiomi T, Okada Y (2003) MT1-MMP and MMP-7 in invasion and metastasis of human cancers. *Cancer Metastasis Rev* 22: 145 – 152
44. Liu B, Sun L, Song E (2013) Non-coding RNAs regulate tumor cell plasticity. *Sci China Life Sci* 56: 886 – 890
45. Sethi N, Kang Y (2011) Unravelling the complexity of metastasis – molecular understanding and targeted therapies. *Nat Rev Cancer* 11: 735 – 748
46. Rinaldi C, Grunseich C, Sevrioukova IF, Schindler A, Horkayne-Szakaly I, Lamperti C, Landoure G, Kennerson ML, Burnett BG, Bonnemann C *et al* (2012) Cowchock syndrome is associated with a mutation in apoptosis-inducing factor. *Am J Human Genetics* 91: 1095 – 1102
47. Ghezzi D, Sevrioukova I, Invernizzi F, Lamperti C, Mora M, D'Adamo P, Novara F, Zuffardi O, Uziel G, Zeviani M (2010) Severe X-linked mitochondrial encephalomyopathy associated with a mutation in apoptosis-inducing factor. *Am J Human Genet* 86: 639 – 649
48. Putz U, Howitt J, Doan A, Goh CP, Low LH, Silke J, Tan SS (2012) The tumor suppressor PTEN is exported in exosomes and has phosphatase activity in recipient cells. *Sci Signal* 5: ra70
49. Hopkins BD, Fine B, Steinbach N, Dendy M, Rapp Z, Shaw J, Pappas K, Yu JS, Hodakoski C, Mense S *et al* (2013) A secreted PTEN phosphatase that enters cells to alter signaling and survival. *Science* 341: 399 – 402
50. Liang H, He S, Yang J, Jia X, Wang P, Chen X, Zhang Z, Zou X, McNutt MA, Shen WH *et al* (2014) PTENalpha, a PTEN isoform translated through alternative initiation, regulates mitochondrial function and energy metabolism. *Cell Metab* 19: 836 – 848
51. Wegrzyn J, Potla R, Chwae YJ, Sepuri NB, Zhang Q, Koeck T, Derecka M, Szczepanek K, Szelag M, Gornicka A *et al* (2009) Function of mitochondrial Stat3 in cellular respiration. *Science* 323: 793 – 797
52. Vaseva AV, Marchenko ND, Ji K, Tsirka SE, Holzmann S, Moll UM (2012) p53 opens the mitochondrial permeability transition pore to trigger necrosis. *Cell* 149: 1536 – 1548
53. Naguib A, Bencze G, Cho H, Zheng W, Tocilj A, Elkayam E, Faehnle CR, Jaber N, Pratt CP, Chen M *et al* (2015) PTEN functions by recruitment to cytoplasmic vesicles. *Mol Cell* 58: 255 – 268
54. Papa A, Wan L, Bonora M, Salmena L, Song MS, Hobbs RM, Lunardi A, Webster K, Ng C, Newton RH *et al* (2014) Cancer-associated PTEN mutants act in a dominant-negative manner to suppress PTEN protein function. *Cell* 157: 595 – 610
55. Liu CX, Yin QQ, Zhou HC, Wu YL, Pu JX, Xia L, Liu W, Huang X, Jiang T, Wu MX *et al* (2012) Adenanthin targets peroxiredoxin I and II to induce differentiation of leukemic cells. *Nat Chem Biol* 8: 486 – 493
56. Rhee SG, Woo HA (2011) Multiple functions of peroxiredoxins: peroxidases, sensors and regulators of the intracellular messenger H_2O_2, and protein chaperones. *Antioxid Redox Signal* 15: 781 – 794
57. Yang L, Lin C, Liu ZR (2006) P68 RNA helicase mediates PDGF-induced epithelial mesenchymal transition by displacing Axin from beta-catenin. *Cell* 127: 139 – 155
58. Damsky WE, Curley DP, Santhanakrishnan M, Rosenbaum LE, Platt JT, Gould Rothberg BE, Taketo MM, Dankort D, Rimm DL, McMahon M *et al* (2011) beta-catenin signaling controls metastasis in Braf-activated Pten-deficient melanomas. *Cancer Cell* 20: 741 – 754
59. Urbano A, Lakshmanan U, Choo PH, Kwan JC, Ng PY, Guo K, Dhakshinamoorthy S, Porter A (2005) AIF suppresses chemical stress-induced apoptosis and maintains the transformed state of tumor cells. *EMBO J* 24: 2815 – 2826
60. Lee JW, Jeong EG, Soung YH, Kim SY, Nam SW, Kim SH, Lee JY, Yoo NJ, Lee SH (2006) Immunohistochemical analysis of apoptosis-inducing factor (AIF) expression in gastric carcinomas. *Pathol Res Pract* 202: 497 – 501
61. Jeong EG, Lee JW, Soung YH, Nam SW, Kim SH, Lee JY, Yoo NJ, Lee SH (2006) Immunohistochemical and mutational analysis of apoptosis-inducing factor (AIF) in colorectal carcinomas. *APMIS* 114: 867 – 873
62. Chiang YY, Chow KC, Lin TY, Chiang IP, Fang HY (2014) Hepatocyte growth factor and HER2/neu downregulate expression of apoptosis-inducing factor in non-small cell lung cancer. *Oncol Rep* 31: 597 – 604
63. Yu Y, Wang LS, Shen SM, Xia L, Zhang L, Zhu YS, Chen GQ (2007) Subcellular proteome analysis of camptothecin analogue NSC606985-treated acute myeloid leukemic cells. *J Proteome Res* 6: 3808 – 3818
64. Morand JP, Macri J, Adeli K (2005) Proteomic profiling of hepatic endoplasmic reticulum-associated proteins in an animal model of insulin resistance and metabolic dyslipidemia. *J Biol Chem* 280: 17626 – 17633
65. Klotz AV, Stegeman JJ, Walsh C (1984) An alternative 7-ethoxyresorufin O-deethylase activity assay: a continuous visible spectrophotometric method for measurement of cytochrome P-450 monooxygenase activity. *Anal Biochem* 140: 138 – 145
66. Shen SM, Yu Y, Wu YL, Cheng JK, Wang LS, Chen GQ (2010) Downregulation of ANP32B, a novel substrate of caspase-3, enhances caspase-3 activation and apoptosis induction in myeloid leukemic cells. *Carcinogenesis* 31: 419 – 426
67. Zhou A, Carrell RW, Murphy MP, Wei Z, Yan Y, Stanley PL, Stein PE, Broughton Pipkin F, Read RJ (2010) A redox switch in angiotensinogen modulates angiotensin release. *Nature* 468: 108 – 111